

# Subaru/HDS Abundances in Three Giant Stars in the Ursa Minor Dwarf Spheroidal Galaxy \*

Kozo SADAKANE

*Astronomical Institute, Osaka Kyoiku University, Kashiwara-shi, Osaka 582-8582*  
*sadakane@cc.osaka-kyoiku.ac.jp*

Nobuo ARIMOTO, Chisato IKUTA, Wako AOKI

*National Astronomical Observatory, 2-21-1 Osawa, Mitaka, Tokyo 181-8588*

Pascale JABLONKA

*Observatoire de Paris, 5 place Jules Janssen, F-92195 Meudon Cedex, France*  
and

Akito TAJITSU

*Subaru Telescope, National Astronomical Observatory of Japan, 650 North A'ohoku Place,  
Hilo, HI96720, USA*

(Received 2004 April 19; accepted 2004 October 27)

## Abstract

With the HDS (High Dispersion Spectrograph) on the Subaru telescope, we obtained high resolution optical region spectra of three red giant stars (cos 4, cos 82, and cos 347) in the Ursa Minor dwarf spheroidal galaxy. Chemical abundances in these stars have been analysed for 26 elements including  $\alpha$ –, iron–peak, and neutron capture elements. All three stars show low abundances of  $\alpha$ –elements (Mg, Si, and Ca) and two stars (cos 82 and cos 347) show high abundance of Mn compared to Galactic halo stars of similar metallicity. One star (cos 4) has been confirmed to be very metal deficient ( $[\text{Fe}/\text{H}] = -2.7$ ) and found to show anomalously low abundances of Mn, Cu, and Ba. In another star cos 82 ( $[\text{Fe}/\text{H}] = -1.5$ ), we have found large excess of heavy neutron-capture elements with the general abundance pattern similar to the scaled solar system  $r$ –process abundance curve. These observational results are rather puzzling: low abundances of  $\alpha$ –elements and high abundance of Mn seem to suggest a significant contribution of SNe Ia at low metallicity, while there is no hint of  $s$ –process (i.e., AGB stars) contribution even at  $[\text{Fe}/\text{H}] = -1.5$ , suggesting a peculiar nucleosynthetic history of the UMi dSph galaxy.

**Key words:** Stars:abundances — Galaxies:abundances —Galaxies: dwarf —Galaxies individual:Ursa Minor

## 1. Introduction

The origin of the Galactic dwarf spheroidal (dSph) galaxies is closely related to the formation and evolutionary history of the Milky Way. Modern cosmological models based on the Cold Dark Matter paradigm demonstrate the importance of hierarchical structure formation on all scales. Galaxies like the Milky Way and M31 form as part of a local overdensity in the primordial matter distribution via the agglomeration of numerous smaller building blocks which independently can develop into dwarf galaxies. In the Local Group the leftovers of this process are seen in the distribution and properties of the dwarf galaxies, with the dwarf spheroidals found mainly close in to the giant spirals, while the dwarf irregulars are more evenly distributed throughout the Local Group.

The gravitationally bound dwarf galaxies that have managed to avoid tidal destruction and subsequent merging have undergone episodic star formation over a Hubble time. The relatively gas-rich dwarf irregulars still exhibit

ongoing star formation, while the dwarf spheroidals, being devoid of significant amounts of gas and dust, are now quiescent and are therefore, in principle, much simpler systems to study. The proximity of the Galactic dSphs offers a unique opportunity for investigating galaxy formation and evolution in unprecedented detail by studying the photometric and spectroscopic properties of the dSph stellar populations.

In this respect, an important approach is to explore the chemical abundances in individual stars belonging to nearby dSph galaxies and to compare them with abundances found in Galactic halo stars. Recently, various nearby dSph galaxies have been the subject of extensive studies concerning accurate abundance analyses based on high dispersion spectroscopic observations using ground-based 8-m class telescopes.

Shetrone et al. (1998) analysed high resolution spectra of four red giant stars in the Draco dSph galaxy observed with the KECK HIRES spectrograph. Smecker-Hane and McWilliam (1999) reported preliminary abundances in 14 stars in the Sagittarius dSph galaxy. Bonifacio et al. (2000) obtained high resolution data of two giant stars in the Sgr dSph galaxy using the UVES spectrograph

\* Based on data collected at Subaru Telescope, which is operated by the National Astronomical Observatory of Japan.

on the ESO 8.2 m Kueyen telescope (VLT). Bonifacio et al. (2004) analysed high resolution data of 10 giant stars in the Sgr dSph galaxy and obtained abundances of O, Mg, Si, Ca and Fe. They concluded that a substantial metal rich population exists in the Sgr dSph. High dispersion data of a total of 13 giant stars in Draco, Ursa Minor and Sextans dSph galaxies were analysed by Shetrone et al. (2001). They found large internal dispersions in metallicity of all three galaxies. They also found that the relative abundances of  $\alpha$ -elements,  $[\alpha/\text{Fe}]$ , are lower in dSph galaxies compared with those found in the halo field stars over the same range in metallicity, which hints a non-negligible contribution of Type Ia Supernovae (SN Ia) during early stage of chemical enrichment, but the number of stars observed is too small to conclude. Shetrone et al. (2003) and Tolstoy et al. (2003) carried out extensive abundance analyses of 15 red giant stars in the Sculpter, Fornax, Carina, and Leo I dSph galaxies and discussed the implications for understanding the history of galaxy formation. Shetrone et al. (2003) found that certain abundance patterns appear to be very similar between these four dSph galaxies and Ursa Minor, Draco, Sextans, and Sagittarius dSph galaxies examined in the literature; i.e., iron—peak elements, second  $s$ - and  $r$ -process elements all show Galactic halo-like patterns. The  $\alpha$ -elements, however, can vary from galaxy to galaxy. Sculpter, Leo I, Sextans, Ursa Minor, and Sagittarius dSph galaxies show a slightly decreasing  $[\alpha/\text{Fe}]$  pattern with increasing metallicity, while Fornax and Draco show roughly constant  $[\alpha/\text{Fe}]$ . No uniform picture for nucleosynthesis in dSph galaxies yet appeared, and clearly more abundance data are desperately required.

In order to investigate in more detail the abundance patterns in giant stars of northern dSph galaxies, we have initiated a program to observe high resolution spectra of bright stars in the Ursa Minor dSph galaxy in 2001. The previous study for this galaxy by Shetrone et al. (2001) was based on rather low S/N ( $\sim 30$ ) spectra. We obtained high resolution spectra with higher quality (S/N > 50) using the Subaru Telescope to confirm the previous study and investigate the chemical composition in more detail. In this paper, we report abundance analyses of three stars observed in 2002.

## 2. Observational Data

Spectroscopic observations of three target stars (cos 4, cos 82, and cos 347; designations are taken from Cudworth et al. (1986)) and one reference star (M92-III-13, a member of the globular cluster M92) were carried out with the Subaru telescope using the High Dispersion Spectrograph (HDS) on 2002 May 16 and 17. Figures 1 and 2 show our three target stars on the sky and on the color-magnitude diagram (CMD) of the UMi dSph galaxy. These target stars are located near the tip of the red giant branch of the UMi dSph galaxy and show somewhat peculiar color indices. Two stars (cos 82 and cos 347) are slightly redder while cos 4 is slightly bluer than the mean locus, suggest-

ing that they might represent higher or lower metallicities with respect to the mean of the red giants in the UMi dSph galaxy. Data of two additional reference stars (BD +30°2611 and HD 216143) were obtained on 2001 June 3 using the same instrumental setup. These reference stars were selected from a list of well studied and relatively bright metal deficient giant stars (Burris et al. 2000). All of our reference stars are cooler than 4500 K in  $T_{\text{eff}}$ , have  $\log g$  values smaller than 1.0, and their metallicity,  $[\text{Fe}/\text{H}]$ , range from -1.4 to -2.5.

The echelle grating of this spectrograph is a mosaic of two  $31.6 \text{ gr mm}^{-1}$  gratings, and the dispersion is  $1 \text{ \AA mm}^{-1}$  at  $4300 \text{ \AA}$ . The detector is a mosaic of two  $4k \times 2k$  EEV CCD's with  $13.5 \mu\text{m}$  pixels. We used a slit width of  $1''.0$  ( $0.5 \text{ mm}$ ) and the  $2 \times 2$  binning mode, which enabled us to achieve a spectral resolution of about 45000 by a 3.5 pixels sampling. Technical details and the performance of the spectrograph are described in Noguchi et al. (2002). Our observations covered the wavelength region from  $4400 \text{ \AA}$  to  $7160 \text{ \AA}$  with a gap between  $5720 - 5800 \text{ \AA}$ . Multiple exposures of 1800 sec were obtained for our target stars. The journal of our observation is given in table 1. For flat-fielding of the CCD data, we obtained Halogen lamp exposures (flat images) with the same setup as that for the object frames.

The reduction of two-dimensional echelle spectral data (bias subtraction, flat-fielding, scattered-light subtraction, extraction of spectral data, and wavelength calibration) was performed using the IRAF software package in a standard manner. Spectral data extracted from multiple object images were averaged in order to improve the signal-to-noise (S/N) ratio. The wavelength calibration was done using the Th-Ar comparison spectra obtained during the observations. The measured FWHM of the weak Th lines is  $0.13 \text{ \AA}$  at  $6000 \text{ \AA}$ , and the resulting resolution is around 46000. The S/N ratios of the resulting spectra were measured at several continuum windows between  $6100 \text{ \AA}$  and  $6200 \text{ \AA}$ . The averaged S/N ratio (per pixel) ranges from 50 to 60 for three UMi stars. Those of the comparison stars are between 190 and 360 in the same wavelength region. Measurements of radial velocities of three UMi stars were carried out using the D lines of Na I. All three UMi stars show large negative velocities (ranging from  $-235$  to  $-255 \text{ km s}^{-1}$ ), consistent with the mean value of the six UMi stars given in Shetrone et al. (2001).

In order to illustrate the quality of our data, a small section of the spectra of three target stars together with three reference stars covering the region between  $6160 \text{ \AA}$  and  $6171 \text{ \AA}$  is shown in figure 3. In this region, we find five Ca I lines as well as a Na I line at  $6160.75 \text{ \AA}$ . Additionally, we find a Pr II line at  $6165.89 \text{ \AA}$  in cos 82 and cos 347, which is not visible in the reference stars. We identify an Er II line at  $6170.06 \text{ \AA}$  in cos 82. On the other hand, we notice only one line (Ca I  $6162.18 \text{ \AA}$ ) in cos 4, which suggests that the star is very metal deficient.

### 3. Abundance Analysis

#### 3.1. Line Identification and EW Measurement

In order to prepare a list of absorption lines to be used in abundance analyses, we first registered all symmetric and clean lines observed in the spectrum of the reference star BD +30°2611 between 4600 and 7100 Å. We do not use the spectral region below 4600 Å, because the S/N ratio of the data of UMi stars become very low in the region. Next, we tried to find unblended absorption lines consulting the line list of Kurucz and Bell (1995). In the process, we use the spectrum synthesis program SPTOOL developed by Y. Takeda (private communication) which incorporates the line list and can simulate any required spectral segment using an appropriate model atmosphere for any combination of assumed abundances. As a result, we prepared a list of about 700 clean absorption lines which includes 27 chemical elements (from O to rare earths). The list contains 260 Fe I lines together with many lines of other iron peak elements such as Cr I and Ni I. Nine rare earth elements (from La to Er) are included in the list. Then, we examined the spectra of three UMi stars comparing with the list of BD +30°2611 and selected lines to be measured in each star. In this process, we noticed that lines of heavy rare earth elements (Eu, Gd, Dy, and Er) are extraordinarily strong in cos 82 as illustrated in figure 3. Shetrone et al. (2001) found a very large abundance of Eu in this star (star 199 in their table 4C), but no abundances were reported for Gd, Dy, and Er. Equivalent widths were measured with the program SPTOOL using a Gaussian fitting technique. Equivalent widths measured in the present analysis for two stars (cos 347 and HD 216143) are compared with published data in figure 4. For cos 347, our results are compared with those given in Shetrone et al. (2001). Results for HD 216143 are compared with data given in Johnson (2002). In both cases, we can find no systematic trend or offset. The scatter in the comparison of cos 347 is very large compared to that in the case of HD 216143. The difference clearly demonstrates the effect of the S/N ratio on the equivalent width measurements.

#### 3.2. Atmospheric Parameters and the Fe Abundance

Atmospheric parameters ( $T_{\text{eff}}$ ,  $\log g$ ,  $\xi_t$ , and  $[\text{Fe}/\text{H}]$ ) for each program star have been determined spectroscopically based on the equivalent widths for a set of selected Fe I and Fe II lines. We use in the present analyses those lines listed in the tables of critically evaluated  $\log gf$  values given in Lambert et al. (1996). Measured equivalent widths of Fe I and Fe II lines used in the analyses are given in table 2. Interpolating model atmospheres given in Kurucz (1993), we tried to find a solution for each star which satisfies the following three requirements simultaneously.

- (1) the abundances derived from selected Fe I lines should not show any dependence on the lower excitation potential ( $\chi$ ) (excitation equilibrium),
- (2) the averaged abundances derived from Fe I and Fe II lines should be equal (ionization equilibrium), and

- (3) the abundance derived from Fe I lines should show no dependence on the equivalent width (matching of the shape of the curve-of-growth, i.e., independence on the equivalent widths).

For each of our target and reference stars, we constructed diagrams such as shown in figure 5 (for HD216143) and figure 6 (for cos 4) in order to examine the relations between the Fe abundance and the observed equivalent widths and the lower excitation potential ( $\chi$ ). We repeated calculations changing the relevant parameters until we obtain a satisfactory fulfillment of the above three requirements. In the process, we used only those lines with equivalent widths smaller than 200 mÅ for each star. Resulting parameters for six stars are summarized in table 3. Uncertainties in  $T_{\text{eff}}$ ,  $\log g$ , and  $\xi_t$  are estimated from these diagrams, while that in  $[\text{Fe}/\text{H}]$  is the rms scatter in the derived abundances. We list previously published data of atmospheric parameters for five stars in table 4. Comparing these two tables, we generally find good agreements in the obtained Fe abundances. Shetrone et al. (2001) obtained parameters ( $T_{\text{eff}}$ ,  $\log g$ ,  $\xi_t$ , and  $[\text{Fe}/\text{H}]$ ) for the two common stars in the UMi dSph galaxy (cos 82 and cos 347) using nearly the same method as in our analysis. Their results are in agreements with ours within the expected errors including the reference star M92-III-13.

We find that one of the UMi stars, cos 4, is very metal poor ( $[\text{Fe}/\text{H}] = -2.7$ ). This star is analysed for the first time in our analysis. This is the most metal-poor star found in UMi to date. Shetrone et al. (2001) found similarly metal-deficient stars in Draco (star 119,  $[\text{Fe}/\text{H}] = -2.97$ ) and Sextans (S49,  $[\text{Fe}/\text{H}] = -2.85$ ) dSph galaxies. There is no object with such a low metallicity in Carina, Sculptor, Fornax, and Leo I dSph galaxies analysed by Shetrone et al. (2003). Thus, the UMi star cos 4 is one of the lowest metallicity objects found in dSph galaxies so far.

#### 3.3. Elemental Abundances

Abundances of elements other than Fe have been obtained starting from the list of unblended lines prepared for BD +30°2611. Only those lines for which we can find reliable data of transition probabilities ( $\log gf$  values) were selected from this list to be used in abundance analyses. Generally, we prefer to use  $\log gf$  values given in the home page of NIST Atomic Spectra Database of the National Institute of Standards and Technology (NIST 2003), or in the VALD atomic line database (Kupka et al. 1999). When we can find data in both sources, we use data given in the NIST database. For Si and several heavy elements, we use new  $\log gf$  values found in recent papers. We use  $\log gf$  values given by Bodaghee et al. (2003) for Si I, Lawler et al. (2001a) for La II, Biémont et al. (2002) for Ce II, Biémont et al. (1989) for Sm II, and Lawler et al. (2001b) for Eu II.

Measured equivalent widths of absorption lines other than Fe are listed in table 5 together with adopted  $\log$

*gf* values and their sources. Averaged abundances of 26 elements in our six target stars are summarized in table 6.

### 3.3.1. Light Elements

For the light element Na, we use equivalent widths of two subordinate lines (5682.63 Å and 5688.21 Å) and the D lines to obtain the abundances. The damping constants of the D lines are taken from the VALD atomic line database (Kupka et al. 1999). In cos 4 and cos 82, we could use only the D lines, because the subordinate lines were found to be too weak. The derived abundances of Na ( $[\text{Na}/\text{Fe}]$ ) in our target stars are generally negative (under-abundant) except for the reference star M92-III-13. In cos 82, we find a significant underabundance of Na,  $[\text{Na}/\text{Fe}] = -1.11$ . The abundances of Mg are obtained from only one line of Mg I at 5528.41 Å. The resulting abundance of Mg ( $[\text{Mg}/\text{Fe}]$ ) ranges from +0.4 to +0.7 dex in the reference stars, while it ranges from +0.1 to +0.4 dex in three UMi stars. Thus, we find a slight under-abundance of Mg in UMi stars when compared to our reference stars. We use two weak lines of Si I to obtain the abundance of Si. For these lines, we adopt recently published solar log *gf* values given in Bodaghee et al. (2003). The resulting abundances of Si ( $[\text{Si}/\text{Fe}]$ ) show solar values except for cos 4, in which we find an over-abundance,  $[\text{Si}/\text{Fe}] = +0.66$ . Considering the weakness of the Si I lines and the relatively poor S/N ratio for cos 4, the apparent over-abundance of Si in this star should be interpreted with caution. For Ca, we measured equivalent widths of at least 12 Ca I lines. The resulting abundances of Ca ( $[\text{Ca}/\text{Fe}]$ ) in UMi stars show no significant differences from the reference stars. Shetrone et al. (2001) noted that all their sample stars belonging to three dSph galaxies show a statistically significant under-abundances of Mg and Ca when compared with Galactic halo stars with the same metallicity. They obtained a mean value of  $[\alpha/\text{Fe}]$  of  $+0.13 \pm 0.04$  for UMi dSph stars. They noted that the mean value of  $[\alpha/\text{Fe}]$  for halo field stars over the same metallicity range is  $+0.28 \pm 0.02$  dex. We obtained from our three UMi stars a mean value of  $[\alpha/\text{Fe}]$  to be +0.16, which is nearly coincident with the result of Shetrone et al. (2001).

### 3.3.2. Iron Peak Elements

For V, Cr, Co, and Ni, our results of abundances ( $[\text{X}/\text{Fe}]$ ) in three UMi stars do not show significant differences from the three reference stars. The abundances of Mn are determined from equivalent widths of nine Mn I lines. We find that the Mn I lines are strikingly weak in cos 4. In figure 7, we compare the strongest line of Mn I in cos 4, cos 347, and BD +30°2611. The Mn I line at 5394.68 Å is fairly strong in the latter two objects, while the line is invisible in cos 4. Assuming an upper limit of the equivalent width of the Mn I line to be 10 mÅ, we estimate the upper limit of the abundance of Mn in cos 4 to be  $[\text{Mn}/\text{Fe}] \leq -0.70$ . The abundance of Mn found in cos 4 is lower than in any other dSph stars analysed by Shetrone et al. (2001). We can find no dSph object

which shows such a low abundance of Mn in Shetrone et al. (2003), either.

The abundances of Cu are obtained from the Cu I line at 5105.54 Å. The Cu I line in cos 4 is compared with those observed in cos 347 and BD°+30 2611 in figure 8. We find that the Cu I line at 5105.54 Å is invisible in cos 4. From an estimated upper limit of the equivalent width (10 mÅ) of the line, we obtain the upper limit of the Cu abundance in cos 4 to be  $[\text{Cu}/\text{Fe}] \leq -0.76$ . The upper limit of Cu found for cos 4 is among the lowest values found in Shetrone et al. (2001).

### 3.3.3. Heavy Elements

From the measured equivalent widths of two Y II lines, we find a low abundance of Y in cos 4,  $[\text{Y}/\text{Fe}] = -0.56$ . The abundances of Y found in cos 82 and in cos 347 are in agreement with results given in Shetrone et al. (2001). We obtain a high abundance of Zr in cos 82 from the Zr II line at 5112.28 Å. No data of the Zr abundances in dSph stars are given in Shetrone et al. (2001), nor in Shetrone et al. (2003). The abundances of Zr ( $[\text{Zr}/\text{Fe}]$ ) in three reference stars are found to coincide with the solar value.

We use three Ba II lines in deriving the abundances of Ba. The Ba II line at 6496.90 Å in three stars (cos 4, cos 82 and cos 347) is compared with that in the reference star BD°+30 2611 in figure 9. We notice that the Ba II line is very weak in cos 4. The resulting abundance of Ba in cos 4 is  $[\text{Ba}/\text{Fe}] = -1.28$ , which is the lowest abundance of Ba in all dSph stars analysed by Shetrone et al. (2001).

Absorption lines of nine rare earth elements (La through Er) have been surveyed in our three dSph stars. We could identify and measure only two weak lines of Nd II in cos 4. On the other hand, we identified absorption lines of heavy rare earths Gd ( $Z = 64$ ), Dy ( $Z = 66$ ), and Er ( $Z = 68$ ) in cos 82. Figure 10 shows the identification of the Dy II line at 5090.39 Å in cos 82. Although the Dy II line is weakly visible in the reference star BD +30°2611, the line is extraordinarily strong in cos 82. Each three Gd II and Er II lines are clearly identified in cos 82, and abundances of these heavy rare earth elements have been determined for the first time in this star.

For several odd- $Z$  rare earth elements such as La, Pr and Eu, we have to take the effects of hyper-fine splitting (hfs) into account in abundance determinations. Data of hfs for La II, Pr II, and Eu II lines were provided by Lawler et al. (2001a), Aoki et al. (2001), and Lawler et al. (2001b), respectively. For each line of these elements, we computed curves of growth with and without the effect of hfs for each target star. Then, the necessary correction factors have been evaluated and applied to each line to obtain the final abundances. When a line has a large splitting and large observed equivalent width (stronger than 120 mÅ), a correction factor as large as  $-0.9$  dex has to be applied.

## 4. Discussion

Two stars (cos 82 = 199; cos 347 = 297) are common in Shetrone et al. (2001) and our sample. Both analyses give very similar abundances for iron and  $\alpha$ -elements



and show no sign of systematic difference, confirming basic results of Shetrone et al. (2001), although the signal-to-noise ratio are not exactly the same. In figure 11, [Ca/Fe] and [Mn/Fe] for three stars (cos 4, cos 82, cos 347) are plotted against [Fe/H], together with four stars (177, K, O, 168) taken from Shetrone et al. (2001). We find that [Ca/Fe] of UMi dSph stars are systematically lower than Galactic metal-poor stars at [Fe/H] < -1.5. This could be explained 1) if SNe Ia contributed in much earlier stage of chemical enrichment (due to lower SFR) and/or 2) if a later stage of small star formation events had fewer high-mass Type II Supernovae (SNe II), thus resulting in lower [Ca/Fe] values as suggested by Shetrone et al. (2003). Taking the decline of [Ca/Fe] in Ursa Minor dSph galaxy as a sign of SNe Ia explosions, Ikuta and Arimoto (2002) claimed that the SFR should be 20 – 40 times lower than that in the solar neighbourhood, if the Salpeter initial mass function is assumed. With such a very low SFR, the star formation should last at least 4 – 6 Gyrs in order to explain the observed metallicities in cos 82 ([Fe/H] = -1.51) and cos 347 ([Fe/H] = -1.67) derived in this study.

Mn is supposed to come from SNe Ia (e.g., Nakamura et al. 1999), thus its abundance would provide a crucial test for distinguishing the two cases given above. We find that both cos 82 ([Mn/Fe] = -0.15) and cos 347 ([Mn/Fe] = +0.05) show noticeable enhancement of Mn with respect to the Galactic halo stars of similar metallicity, which may suggest that SNe Ia had contributed already significantly at this early stage of chemical enrichment. We should point out that cos 4 is enriched in Mg ([Mg/Fe] = 0.31), Si ([Si/Fe] = 0.66), and Ca ([Ca/Fe] = 0.21), while showing considerably low Mn abundance ([Mn/Fe] < -0.70), implying that SNe Ia had little contribution at this very beginning of the enrichment.

If the star formation has been inefficient as suggested by Ikuta and Arimoto (2002), the chemical enrichment in Ursa Minor dSph, or in dSph galaxies in general, might have been inhomogeneous and the observed stars may reflect the local enrichment due to particular supernovae exploded in the vicinity of these stars. We have compared the abundance patterns of cos 4, cos 82, and cos 347 from Mg to Zn with metal-poor stars ( $-2 < [\text{Fe}/\text{H}] < -1$ ; Gratton 1989; Sneden et al. 1991; Gratton and Sneden 1988; Gratton and Sneden 1991; Gratton and Sneden 1994; Edvardsson et al. 1993; McWilliam et al. 1995; Nissen and Schuster 1997; Stephens 1999) and extremely metal-poor stars ( $-4 < [\text{Fe}/\text{H}] < -2$ ; Cayrel et al. 2004) in the Milky Way. We may conclude that there is no clear sign for the influence of local supernovae explosions in the abundance patterns from Mg to Zn in these three stars: 1) [Na/Fe], [Mg/Fe], [Si/Fe], [Ca/Fe], and [Cr/Fe] of cos 4 are normal at [Fe/H] = -2.7. On the other hand, [Ti/Fe] and [Mn/Fe] are definitely lower in cos 4 than in the Galactic metal-poor giants. [Ni/Fe] and [Zn/Fe] in cos 4 are also slightly lower than the Galactic mean values at [Fe/H] = -2.7. 2) cos 82 and cos 347 show very similar abundance patterns to each other. With respect to the metal-poor stars in the Milky Way, these stars have

similar values of [Mg/Fe], [Co/Fe], [Ni/Fe], [Cu/Fe], and [Zn/Fe], but significantly lower values of [Si/Fe], [Ca/Fe], and [Ti/Fe]. [Cr/Fe] and [Mn/Fe] are enhanced and are close to the disc stars of higher metallicity ([Fe/H] > -1). The abundance patterns from Mg to Zn suggest that SNe Ia had already contributed significantly to the enrichment before cos 82 and cos 347 were formed. We therefore tentatively conclude that the three stars we observed were not affected by local supernovae explosions, instead they all keep the record of global enrichment history of Ursa Minor dSph.

Figure 12 shows relative abundances of neutron capture elements (Y through Er) in the heavy element-enhanced stars cos 82 ([Eu/Fe] = 0.97) and cos 347 ([Eu/Fe] = 0.61). We compare the observed abundance patterns with the solar-system *r*-process and *s*-process abundance patterns. We take the total solar-system abundances from Grevesse and Sauval (1998) and use the *r*-process and *s*-process fractions in the solar-system given by Burris et al. (2000). Surprisingly, we find that the general features of heavy rare earth elements agree quite well with the scaled solar system *r*-process abundance curve. The agreement of the abundance pattern with that of the solar system *r*-process component was already suggested by Shetrone et al. (2001), but our study clearly confirms this including the heavier elements Gd, Dy, and Er. This implies that the heavy rare earth elements of these stars are of *r*-process origin, and the contribution from the *s*-process is still considerably small, even though the metallicities of these stars are remarkably high. The abundance patterns of heavy rare earth elements are very close to that of Galactic metal-poor stars, in particular, we find the ratio [Ba/Eu] = -0.59 and -0.43 for cos 82 and cos 347, respectively, again showing that the ratios are clearly associated with the *r*-process (as is shown in McWilliam (1998)), rather than the *s*-process, although the contribution from the *s*-process may not be negligible in cos 347.

The abundance patterns of individual elements prevent us from deriving a fully consistent picture of chemical enrichment in the Ursa Minor dSph galaxy: low abundances of  $\alpha$  - elements and high abundance of Mn imply a significant contribution from SNe Ia (lifetime of the progenitor  $\sim 10^9$  yrs) at low metallicity ([Fe/H] < -1.5), suggesting rather long period of star formation with very low SFR. On the other hand, the contribution from the *s*-process (i.e., from AGB stars of lifetime  $\sim 10^8$  yrs) is still considerably small even at [Fe/H] = -1.5, which seems to suggest that the time scale of star formation in the Ursa Minor dSph galaxy is very short. The latter possibility was proposed by Tsujimoto and Shigeyama (2002). If one assumes that there are two distinct classes of massive supernovae – one produces and ejects *r*-process elements and the other does not, and if one further assumes that SNe II with the main sequence mass of 20 – 25  $M_{\odot}$  are the dominant site for *r*-process nucleosynthesis (Tsujimoto and Shigeyama 2002), a sharp rise of [Ba/Fe] in dSph galaxies should occur between [Fe/H]  $\sim -2.5$  and  $\sim -2.0$ , which corresponds to massive explosions of these SNe II whose progenitors' lifetimes are an order of a few  $10^7$

years. Unfortunately, very small number of observed stars prevents us from further analysis. A systematic study of extremely metal-deficient stars ( $[\text{Fe}/\text{H}] < -2.0$ ) with much higher signal-to-noise spectra would certainly provide a critical understanding of the early enrichment history of dSph galaxies.

## 5. Summary

Our main findings concerning the abundances of the three UMi dSph stars are as follows.

1. We find a very metal poor star cos 4 in which Fe is more under-abundant than other stars in the UMi dSph analysed so far.
2. In cos 4, we find that three elements Mn, Cu and Ba are extra-ordinarily deficient. The underabundance of Mn implies that SNe Ia had little contribution in this star. Y appears to be under-abundant in this star, too.
3. We find that the light element Na is significantly under-abundant in cos 82.
4. Abundances of  $\alpha$  elements (especially Ca) in cos 82 and cos 347 are found to be lower, while that of Mn in these two stars to be higher than the corresponding values in Galactic metal poor stars.
5. At the same time, we find large excesses of heavy neutron-capture elements in these two stars with the general abundance pattern similar to the scaled solar system  $r$ -process abundance curve.

These results appear to be rather puzzling: low abundances of  $\alpha$  - elements and high abundance of Mn seem to suggest a significant contribution of SNe Ia at  $[\text{Fe}/\text{H}] = -1.5$ , while there is no hint of  $s$ -process (i.e., AGB stars) contribution even at this metallicity, probably suggesting a peculiar nucleosynthesis history of the UMi dSph galaxy.

We thank Dr. A. Schweitzer for providing us with unpublished data of proper motion and photometry of the UMi dSph and also thank all staff members of the Subaru telescope, NAOJ, for their help during the observation. Thanks are also due to M. Ohkubo for her help in preparing the manuscript. This research was partly supported by a Grant-in-Aid, No. 13640230 (to N.A.) and No. 15540236 (to K.S.) from the Ministry of Education, Culture, Sports, Science and Technology, Japan.

## References

- Aoki, W. et al., 2001, *ApJ*, 561, 346  
 Biémont, E., Grevesse, N., Hanaforde, P., & Lowe, R. M. 1989, *A&A*, 222, 307  
 Biémont, E., Palmeri, P., & Quinet, P. 2002, <http://www.umh.ac.be/astro/dream.shtml>  
 Bodaghe, A., Santos, N. C., Israelian, G., & Mayor, M. 2003, *A&A*, 404, 715  
 Bonifacio, P., Hill, V., Molaro, P., Pasquini, L., Di Marcantonio, P., & Santin, P. 2000, *A&A*, 359, 663  
 Bonifacio, P., Sbordone, L., Marconi, G., Pasquini, L., & Hill, V. 2004, *A&A*, 414, 503  
 Burris, D. L., Pilachowski, C. A., Armandroff, T. E., Sneden, C., Cowan, J. J., & Roe, H. 2000, *ApJ*, 544, 302  
 Carretta, E., & Gratton, R. G. 1997, *A&AS*, 121, 95  
 Cayrel, R. et al. 2004, *A&A*, 416, 1117  
 Cudworth, K. M., Olszewski, E. W., & Schommer, R. A. 1986, *AJ*, 92, 766  
 Edvardsson, B., Andersen, J., Gustafsson, B., Lambert, D. L., Nissen, P. E., & Tomkin, J. 1993, *A&A*, 275, 101  
 Francois, P. 1996, *A&A*, 313, 229  
 Fulbright, J.P. 2000, *AJ*, 120, 1841  
 Gratton, R. G. 1989, *A&A*, 208, 171  
 Gratton, R. G. & Sneden, C. 1988, *A&A*, 204, 193  
 Gratton, R. G. & Sneden, C. 1991, *A&A*, 241, 501  
 Gratton, R. G. & Sneden, C. 1994, *A&A*, 287, 927  
 Grevesse, N. & Sauval, A.J. 1998, *Space Science Reviews*, 85, 161  
 Ikuta, C. & Arimoto, N. 2002, *A&A*, 391, 55  
 Johnson, J.A. 2002, *ApJS*, 139, 219  
 Kupka, F., Piskunov, N., Ryabchikova, T. A., Stempels, H. C., & Weiss, W. W. 1999, *A&AS*, 138, 119  
 Kurucz, R. L. 1993, Kurucz CD-ROM, No.13 (Harvard-Smithsonian Center for Astrophysics)  
 Kurucz, R. L. & Bell, B. 1995, Kurucz CD-ROM, No.23 (Harvard-Smithsonian Center for Astrophysics)  
 Lawler, J. E., Bonvallet, G., & Sneden, C. 2001a, *ApJ*, 556, 452  
 Lawler, J. E., Wickliffe, M. E., den Hartog, E. A., & Sneden, C. 2001b, *ApJ*, 563, 1075  
 Lambert, D. L., Heath, J. E., Lemke, M., & Drake, J. 1996, *ApJS*, 103, 183  
 McWilliam, A. 1998, *AJ*, 115, 1640  
 McWilliam, A., Preston, G.W., Sneden, C., & Searle, L. 1995, *AJ*, 109, 2757  
 Mishenina, T. V., & Kovtyukh, V. V. 2001, *A&A*, 370, 951  
 Nakamura, T., Umeda, H., Nomoto, K., Thielemann, F.-K., Burrows, A. 1999, *ApJ*, 517, 193  
 NIST 2003, <http://physics.nist.gov/PhysRefData/contents-atomic.html>  
 Nissen, P. E., & Schuster, W. J. 1997, *A&A*, 326, 751  
 Noguchi, K., et al., 2002, *PASJ*, 54, 855  
 Pilachowski, C. A., Sneden, C., & Kraft, R. P. 1996, *AJ*, 111, 1689  
 Shetrone, M. D. 1996, *AJ*, 112, 1517  
 Shetrone, M. D., Bolte, M., & Stetson, P. B. 1998, *AJ*, 115, 1888  
 Shetrone, M. D., Cote, P., & Sargent, W. L. W. 2001, *ApJ*, 548, 592  
 Shetrone, M., Venn, K. A., Tolstoy, E., Primas, F., Hill, V., & Kaufer, A. 2003, *AJ*, 125, 684  
 Smecker-Hane, T., & McWilliam, A. 1999, in *ASP Conf. Ser.* 192, *Spectrophotometric Dating of Stars and Galaxies*, ed. I. Hubeny, S. R. Heap & R. H. Cornett (San Francisco, ASP), 150  
 Sneden, C., Gratton, R. G., & Crocker, D.A. 1991, *A&A*, 246, 354  
 Sneden, C., Pilachowski, C. A., & Kraft, R. P. 2000, *AJ*, 120, 1351  
 Stephens, A. 1999, *AJ*, 117, 1771  
 Tolstoy, E., Venn, K. A., Shetrone, M., Primas, F., Hill, V., Kaufer, A., & Szeifert, T. 2003, *AJ*, 125, 707



**Table 1.** Observational Log.

Object	$V$	$B - V$	Exposure (Min.)	Obs. Date	SN (per pixel) (at 6100 Å)
HD 216143	7.82	0.94	4	2001, June, 3	350
BD +30°2611	9.14	1.16	10	2001, June, 3	360
M92-III-13	12.03	1.28	20	2002, May, 16	190
cos 347	16.94	1.52	150	2002, May, 16	55
cos 4	16.73	1.33	210	2002, May, 16	50
cos 82	17.2	1.36	180	2002, May, 16, 17	60

**Table 2.** Equivalent widths of Fe I and Fe II lines.

ion	Wavelength (Å)	$\chi$ (eV)	$\log gf$	cos 4	cos 82	cos 347	BD +30°2611	HD 216143	M92-III-13
Fe I	4966.087	3.332	-0.84	40				69	82
	4969.916	4.217	-0.75				69	19	28
	4973.101	3.960	-0.85					27	37
	5002.789	3.396	-1.44					27	40
	5014.941	3.943	-0.27	30	121		106	52	58
	5022.236	3.984	-0.49		91			40	47
	5044.210	2.851	-2.04			111		34	50
	5049.819	2.279	-1.35	88	167		183	108	135
	5051.634	0.915	-2.78	132				134	
	5074.748	4.220	-0.16		166		104	47	58
	5083.338	0.958	-2.91	105	178		183	120	
	5090.767	4.256	-0.36		81	73	82	27	29
	5110.413	0.000	-3.76	156			231	149	
	5121.641	4.283	-0.72				67	16	27
	5125.112	4.220	-0.08	26				50	
	5133.681	4.178	0.20	42	128	127	128	66	78
	5150.838	0.990	-3.00	100	186		187	111	
	5151.910	1.011	-3.32	94				101	
	5159.050	4.283	-0.65		66			13	
	5162.292	4.178	0.08	35	122	100		60	68
	5171.595	1.485	-1.76	147				138	
	5194.941	1.557	-2.06	119			191	122	157
	5198.711	2.223	-2.14	50	145	155	144	77	104
	5202.335	2.176	-1.84					102	134
	5216.274	1.608	-2.12	108	177			119	147
	5232.939	2.940	-0.08	99	188		210	128	150
	5242.491	3.634	-0.97		103		99	37	46
	5250.208	0.121	-4.92	62	153		162	78	136
	5253.023	2.279	-3.79		37	48		4	
	5281.790	3.038	-0.83	48	135	152		84	103
	5288.528	3.695	-1.51		59	51	59	13	18
	5302.299	3.283	-0.74	45				136	70
	5307.360	1.608	-2.97	58	133	168	140	76	105
	5322.041	2.279	-2.84	23	104	109	97	27	50
	5324.178	3.211	-0.10	84	173	185		108	128
	5339.928	3.266	-0.68	41	149	133		76	99
	5341.023	1.608	-1.95	116				132	
	5364.858	4.446	0.23	28	100	94	102	46	64
	5367.479	4.415	0.44	37	105	108	110	54	61
	5369.958	4.371	0.54		117		118	59	72
	5371.489	0.958	-1.65					183	
	5373.698	4.473	-0.71		53		51	10	10
	5383.369	4.312	0.65	43		134	126	69	77
	5389.479	4.415	-0.25					21	24
	5393.167	3.241	-0.72	40		154		77	95
	5400.502	4.371	-0.10		108			33	44
	5405.774	0.990	-1.85	168				169	
	5410.910	4.473	0.40	30	116	103	105	48	54
	5424.069	4.320	0.58	36	136	149	137	74	86
	5429.696	0.958	-1.88	183				180	
	5434.523	1.011	-2.12	163			245	156	
	5445.042	4.386	0.04	18	93	98	98	42	49
	5466.390	4.371	-0.57		60		70	17	22
	5497.516	1.011	-2.84	128				131	
	5506.778	0.990	-2.80	127	196			130	
	5554.882	4.548	-0.38		72			16	
	5567.392	2.608	-2.56	19	102	95	89	20	38
	5569.618	3.417	-0.49	45	150	157	139	74	93
	5572.841	3.396	-0.28	57	170			89	110
	5576.090	3.430	-0.85	35	116	137	121	57	73
	5586.756	3.368	-0.12			168	165	100	118
	5615.644	3.332	0.05					111	134



Table 2. continued.

ion	Wavelength (Å)	$\chi$ (eV)	$\log gf$	cos 4	cos 82	cos 347	BD +30°2611	HD 216143	M92-III-13
Fe I	5618.631	4.209	-1.26				38	7	
	5633.975	4.991	-0.12				43	8	
	5679.025	4.652	-0.77				39	7	11
	5686.524	4.548	-0.45				59	12	18
	5883.813	3.960	-1.21		60	65	65	14	
	5916.249	2.453	-2.99		78	96		20	44
	5934.653	3.929	-1.02			67	76	18	
	6020.170	4.607	-0.21					23	25
	6024.049	4.548	-0.06	16	87	81	93	34	
	6027.050	4.076	-1.09		67	60	63	12	11
	6065.482	2.608	-1.53	50	162	182	156	88	113
	6078.999	4.652	-0.97		27	21	25	3	
	6082.708	2.223	-3.58		67	86	67	11	24
	6136.615	2.453	-1.40	87	173			107	134
	6137.694	2.588	-1.40	64	156	184	174	98	124
	6151.617	2.176	-3.29	13	78	102	90	22	42
	6157.725	4.076	-1.11		76	77	66	13	
	6170.504	4.795	-0.38		49	56		11	17
	6173.341	2.223	-2.88	21	118	132	111	38	69
	6187.987	3.943	-1.57		48	48	43	6	10
	6191.558	2.433	-1.42	79				105	136
	6200.314	2.608	-2.44	17	105	116	108	34	54
	6213.429	2.223	-2.48	30	137	147	132	58	89
	6230.726	2.559	-1.28	83	179		202	110	145
	6252.554	2.404	-1.72	62			166	95	127
	6254.256	2.279	-2.44	38	135	162	143	64	93
	6265.131	2.176	-2.55	39	131	158	136	63	93
	6322.690	2.588	-2.43	25	113	128	112	41	60
	6393.602	2.433	-1.43	79	168	189	172	102	129
	6421.349	2.279	-2.01	55				89	121
	6430.844	2.176	-2.01	67	167	188	172	97	132
	6592.913	2.727	-1.47	57	158	157	151	81	105
	6593.871	2.433	-2.42	44	133	136	125	51	78
	6609.110	2.559	-2.69				100	28	48
	6750.150	2.424	-2.62	29	123	119	115	43	73
	6841.335	4.607	-0.60		41	41	45	11	12
Fe II	5132.669	2.807	-4.00		40		33	11	
	5197.577	3.230	-2.25	50		92	100	66	70
	5234.625	3.221	-2.24	58	113	99	95	70	69
	5276.002	3.199	-1.91	59				87	
	5284.109	2.891	-3.01	19	68	68	67	39	40
	5325.553	3.221	-3.17			54	44	20	20
	5414.073	3.221	-3.62			36	27	8	10
	5425.257	3.199	-3.21	12	40		45	18	19
	5534.847	3.245	-2.77	26	83	65		39	38
	5991.376	3.153	-3.56	...	42			16	
	6084.111	3.199	-3.80	...	24	25	21	7	9
	6149.258	3.889	-2.72	...	32			15	13
	6247.557	3.892	-2.34	...		35	47	25	23
	6369.462	2.891	-4.19	...	33		16	8	
	6432.680	2.891	-3.58	...	47	40	47	22	21

Table 3. Atmospheric parameters.

Object	$T_{\text{eff}}$ (K)	$\log g$	$\xi_t$ (km s <sup>-1</sup> )	[Fe/H]
HD 216143	4450 ± 100	0.8 ± 0.2	1.8 ± 0.2	-2.18 ± 0.11
BD +30°2611	4250 ± 100	0.7 ± 0.2	2.0 ± 0.2	-1.52 ± 0.10
M92-III-13	4200 ± 100	0.5 ± 0.2	1.9 ± 0.2	-2.15 ± 0.13
cos 347	4050 ± 130	0.3 ± 0.3	2.1 ± 0.3	-1.63 ± 0.19
cos 4	4300 ± 130	0.3 ± 0.3	2.0 ± 0.3	-2.66 ± 0.18
cos 82	4300 ± 110	0.3 ± 0.3	2.0 ± 0.3	-1.53 ± 0.18

**Table 4.** Previously published atmospheric parameters.

Object	$T_{\text{eff}}$ (K)	$\log g$	$\xi_t$ (km s <sup>-1</sup> )	[Fe/H]	Reference*
HD 216143	4582	1.46	2.5	-2.24	1
	4525	0.80	1.8	-2.18	2
	4400	0.70	1.80	-2.26	3
	4525	1.0	2.85	-2.1	4
	4525	0.80	1.80	-2.00	5
	4500	1.0	1.60	-2.11	6
	4500	0.70	2.10	-2.10	7
BD +30°2611	4275	0.80	2.1	-1.49	2
	4500	1.4	2.10	-1.2	4
	4275	0.80	2.10	-1.40	5
	4300	0.70	1.60	-1.41	6
M92-III-13	4125	0.75	1.98	-2.17	8
	4180	0.10	2.15	-2.24	9
	4125	0.75	2.00	-2.39	10
	4175	0.20	2.10	-2.28	11
cos 347	4075	0.40	2.30	-1.68	11
cos 82	4325	0.30	1.95	-1.45	11

\* References: 1. Francois (1996), 2. Pilachowski et al. (1996), 3. Shetrone (1996), 4. Fulbright (2000), 5. Burris et al. (2000), 6. Mishenina and Kovtyuk (2001), 7. Johnson (2002), 8. Carretta and Gratton (1997), 9. Shetrone et al. (1998), 10 Sneden et al. (2000), 11. Shetrone et al. (2001)

**Table 5.** Equivalent widths of other elements.

ion	Wavelength (Å)	$\chi$ (eV)	$\log gf$	Ref	cos 4	cos 82	cos 347	BD +30°2611	HD 216143	M92-III-13
Na I	5682.633	2.102	-0.700	1			43	31	8	28
	5688.205	2.104	-0.457	1			59	50	12	47
	5889.951	0.000	0.112	1	186	243	347	293	222	
	5895.924	0.000	-0.191	1	166	233	332	269	196	
Mg I	5528.405	4.346	-0.620	2	64	150	174	182	116	137
Si I	5948.541	5.082	-1.110	3	14	32	41	52	18	
	6155.134	5.619	-0.750	3	11	31	30	35	10	14
Ca I	5261.704	2.521	-0.591	2	22	93	117	98	32	48
	5512.980	2.932	-0.712	2	15	45	60	77	19	26
	5588.749	2.526	0.313	2	52	148	154	149	84	100
	5590.114	2.521	-0.596	2	17	81	97	97	32	47
	5601.277	2.526	-0.552	2		75	95	99	39	47
	6102.723	1.879	-0.793	1	40	133	158	142	75	102
	6122.217	1.886	-0.315	1	73	158	176	176	106	136
	6161.297	2.523	-1.293	2			57	64	12	21
	6162.173	1.899	-0.089	1	84	187	212	195	122	151
	6166.439	2.521	-1.156	2		55	72	68	15	25
	6169.042	2.523	-0.804	2		75	86	93	28	41
	6169.563	2.526	-0.527	2	14	88	103	108	42	60
	6439.075	2.526	0.394	2	66	147	177	164	98	123
	6455.598	2.523	-1.557	2		38	58	55	8	
	6493.781	2.521	0.019	2	24	103	156	137		85
	6499.650	2.523	-0.719	2	13	53	85	94	28	39
	6717.681	2.709	-0.596	2	14	85	111	108	36	48
Sc II	5239.813	1.455	-0.765	2	36	104	84	95	41	60
	5526.790	1.768	0.025	2	52	95	105	110	65	87
	5669.04	1.500	-1.200	2	21		70	54	25	40
	5684.202	1.507	-1.074	2	22		57	64	28	47
	6245.637	1.507	-1.030	2			52	65	24	44
	6279.753	1.500	-1.265	2	6	43	55	46		
	6320.851	1.500	-1.815	2			28	20	6	11
	6604.601	1.357	-1.309	2		65	71	62	21	41
Ti I	4981.732	0.848	0.504	1	74	134	167	168	96	127
	4997.098	0.000	-2.118	1			134	101	22	60
	4999.500	0.826	0.250	1	60	184	203	175	89	119
	5009.646	0.021	-2.259	1		90	115	95	16	48
	5016.162	0.848	-0.574	1	21	98	148	118	40	61
	5020.028	0.836	-0.415	1		94	159	130	49	81
	5022.871	0.826	-0.434	1	35	114	161	126	50	86
	5024.842	0.818	-0.602	1	22	111	140	121	41	78
	5043.588	0.836	-1.733	1		43	82	55	18	19
	5045.416	0.848	-1.998	1		20	?	38	13	13
	5071.472	1.460	-1.063	1			54	44	11	11
	5145.464	1.460	-0.574	1		58	78	63	21	24
	5147.479	0.000	-2.012	1	28		148	115	25	69

Table 5. continued.

ion	Wevelength (Å)	$\chi$ (eV)	$\log gf$	Ref	cos 4	cos 82	cos 347	BD +30°2611	HD 216143	M92-III-13
Ti II	5192.969	0.021	-1.005	1	60	227	247	192	88	133
	5210.386	0.048	-0.883	1	67	151	239	177	83	138
	5219.700	0.021	-2.292	1		62	143	96	13	45
	5426.237	0.021	-3.006	1		44	78	52	4	20
	5460.469	0.048	-2.804	1		42	91	59	6	25
	5471.197	1.443	-1.389	1		14	21	23		
	5953.162	1.887	-0.329	1		31	53	51	10	16
	6064.629	1.046	-1.944	1		20	43	31	3	9
	6091.174	2.267	-0.423	1		20	29	24		4
	6258.104	1.443	-0.355	1		61	100	93	17	39
	6258.709	1.460	-0.240	1		86	146	119	22	51
	6261.101	1.430	-0.479	1		65	121	97	15	37
	6554.224	1.443	-1.219	1		32	54	41	8	
	6556.062	1.460	-1.075	1		33	58	49	3	9
	6599.133	0.900	-2.085	1		29	51	39		9
	5005.157	1.566	-2.544	1	15	46	39	54	23	32
	5013.677	1.582	-1.990	2	36	74	94	83	49	61
	5154.070	1.566	-1.922	1	45	116	129	115	76	87
	5185.913	1.893	-1.345	1	41	91	112	103	67	85
	5336.771	1.582	-1.703	1	74		149	119	84	102
V I	5381.015	1.566	-2.079	1	49		125	107	63	78
	5396.226	1.584	-3.020	2		32	36	34	11	20
	5418.751	1.582	-2.110	2	45	95	92	92	53	68
	6491.561	2.061	-1.793	2	14	41	74	65	31	54
	4851.482	0.000	-1.138	1		66	132	100	12	
	4864.731	0.017	-0.961	1				87	11	36
	4875.493	0.040	-0.806	1		96	116	104	17	45
	6039.722	1.064	-0.651	1		21	32	31		10
	6081.441	1.051	-0.578	1		32	34	34		10
	6090.214	1.081	-0.062	1		41	72	65	7	24
	6135.361	1.051	-0.746	1		24	34	25		5
	6150.157	0.301	-1.787	1		31	57	39	4	7
	6199.197	0.287	-1.285	1		27	63	53	3	12
	6216.354	0.275	-1.292	1		46	81	67	5	16
	6243.105	0.301	-0.978	1		68	104	95	6	28
Cr I	6251.827	0.287	-1.342	1		33	97	56	3	16
	5247.566	0.961	-1.628	1	33	135	156	125	43	64
	5296.691	0.983	-1.407	1	20	138	160	137	53	84
	5300.744	0.983	-2.132	1		91	122	94	18	39
	5329.142	2.913	-0.064	1			64	63	14	18
	5345.801	1.004	-0.979	1	34	178	190	160	78	104
	5348.312	1.004	-1.292	1	32	135		136	60	82
	5409.772	1.030	-0.720	1	61	179	218	188	90	122
	6330.093	0.941	-2.914	1		62	83	59	5	13
	5394.677	0.000	-3.503	1		128	198	157	24	61
Mn I	5420.355	2.143	-1.460	1		67	92	83	9	18

Table 5. continued.

ion	Wevelength (Å)	$\chi$ (eV)	$\log gf$	Ref	cos 4	cos 82	cos 347	BD +30°2611	HD 216143	M92-III-13
Co I	5432.546	0.000	-3.795	1			162	122	13	39
	5470.637	2.164	-1.702	2		38	57	57	6	10
	5516.774	2.178	-1.847	1		29	48	36	4	8
	5537.760	2.187	-2.017	2		40	51	36	4	8
	6013.513	3.072	-0.252	1		56	70	59	10	9
	6016.673	3.073	-0.216	2		65	72	68	13	15
	6021.819	3.075	0.035	1		77	90	80	18	24
	5230.202	1.740	-1.840	1		38	49	49	6	20
	5331.452	1.785	-1.962	1		50	29	42	4	12
	5369.590	1.740	-1.651	1			60	71	10	34
Ni I	6771.033	1.883	-1.969	1		25	49	45	7	17
	5035.357	3.635	0.290	1			82	86	44	49
	5080.528	3.655	0.134	1	27	99	93	109	46	49
	5084.089	3.678	0.034	1	10	40	70	72	31	34
	5146.480	3.706	-0.060	2		62	75	78	29	35
	5578.711	1.676	-2.641	1		94	99	90	24	48
	5587.853	1.935	-2.142	1		101	95	86	26	43
	5592.259	1.951	-2.588	1		71	98	100	26	48
	6314.653	1.935	-1.768	1	17	114	118	95	32	53
	6327.593	1.676	-3.146	1		86	69	72	17	28
Cu I	6586.308	1.951	-2.812	1		67	73	66	15	30
	6643.629	1.676	-2.304	1	35	130	140	137	65	94
	6767.768	1.826	-2.167	1	20	124	134	119	59	82
	5105.537	1.389	-1.505	1		105	112	103	22	49
Zn I	4810.528	4.078	-0.137	2	29	64	61	62	43	36
Y II	4854.863	0.992	-0.383	2	18			88	44	45
	4883.684	1.084	0.071	2		116	87	94	62	63
	5087.416	1.084	-0.156	2	26	110	85	75	47	50
	5509.895	0.992	-1.015	2		102	72	59	20	25
Zr II	5112.279	1.660	-0.590	2		78	31	31	9	13
Ba II	5853.670	0.600	-1.006	1	14		136	126	73	73
	6141.713	0.704	-0.077	1	34	222	196	183	122	126
	6496.897	0.604	-0.376	1	48	218	205	183	122	125
La II	4921.776	0.244	-0.450	4		135	89	91	35	32
	4986.819	0.173	-1.300	4		123	68	48	10	7
	5114.559	0.235	-1.030	4		126	68	60	13	11
	5163.611	0.244	-1.810	4		63	19	17		
	5290.818	0.000	-1.650	4		74	40	26	5	
Ce II	5303.528	0.321	-1.350	4		76		26	6	
	6320.376	0.173	-1.562	2		115	24	33		
	6390.477	0.321	-1.410	4		84	33	26		
	5117.169	1.402	-0.050	5		38	22	10	2	
	5274.229	1.044	0.150	5		93	51	33	7	5
	5330.556	0.869	-0.460	5		50	33	19	2	
	5472.279	1.247	-0.100	5		39	16	10		



Table 5. continued.

ion	Wevelength (Å)	$\chi$ (eV)	$\log gf$	Ref	cos 4	cos 82	cos 347	BD +30°2611	HD 216143	M92-III-13
Pr II	5219.045	0.795	-0.235	1		80		23	5	3
	5259.740	0.630	0.082	1		112	46	27	6	6
	5292.619	0.648	-0.294	1		83	44	24	4	3
	5322.772	0.483	-0.461	2		119	49	32	7	8
	5352.398	0.483	-0.727	2		66	16	13		
Nd II	4943.899	0.205	-1.514	2		64		26	5	4
	4959.119	0.064	-0.916	2		124	83	77	23	30
	4961.387	0.631	-0.850	2		83	57	34	8	7
	4989.950	0.631	-0.624	2		121	78	55	13	
	5033.507	1.136	-0.527	2		65		16	3	4
	5076.580	0.742	-0.386	2		108	63	46	11	7
	5089.832	0.205	-1.098	2		96	41	35	7	4
	5092.794	0.380	-0.609	2	11	106	70	54	17	13
	5132.328	0.559	-0.818	2		69	56	33	7	6
	5212.361	0.205	-0.768	2	12	109	73	58	14	15
	5249.576	0.976	0.094	2		103	73	60	17	18
	5276.869	0.859	-0.393	2		65	33	25	6	
	5306.460	0.859	-0.799	2		75	29	12		
	5311.453	0.986	-0.437	2		87	33	24	5	5
	5314.554	0.986	-1.216	2		34		5		
	5319.815	0.550	-0.152	2		126	80	75	23	20
	5385.888	0.742	-0.860	2		79	26	20	5	
	5431.516	1.121	-0.457	2		44	27	15	4	
	5442.264	0.680	-0.979	2		72		22	6	
	6428.645	0.205	-1.831	2		57	22	12		
	6514.959	0.182	-1.883	2		69	31	10		
	6740.078	0.064	-1.526	2		99	50	28	5	5
	6790.372	0.182	-1.569	2		59	29	12		
Sm II	4815.806	0.185	-0.770	6		105	55	65	12	10
	4948.631	0.544	-0.840	6		92	31	21	5	
Eu II	6437.640	1.320	-0.320	7		80	27	19	5	
	6645.064	1.380	0.120	7		84	47	37	9	4
Gd II	5108.703	1.659	-0.322	2		43		15		
	5140.830	1.575	-0.738	2		32		10		
	5469.713	1.102	-1.540	2		30	6	5		
Dy II	5090.386	0.103	-2.332	2		68	9	22	3	2
	5169.688	0.103	-1.660	2		82	21	21	2	4
Er II	5414.631	0.000	-2.451	2		72		5		
	6006.783	0.000	-2.737	2		31		5		
	6170.064	0.055	-2.769	2		15		1		

References: 1. NIST (2003) 2. Kupka et al. (1999) 3. Bodaghee et al. (2003) 4. Lawler et al. (2001a) 5. Biémont et al. (2002) 6. Biémont et al. (1989) 7. Lawler et al. (2001b)

**Table 6.** Abundances in Target Stars.

	cos 4			cos 82			cos 347		
	S.D.		N	S.D.		N	S.D.		N
[Fe I/H]	-2.65	0.15	61	-1.51	0.22	63	-1.67	0.14	58
[Fe II/H]	-2.70	0.17	6	-1.55	0.17	10	-1.53	0.16	9
[Na/Fe]	-0.25		2	-1.11		2	-0.27	0.17	4
[Mg/Fe]	0.31		1	0.14		1	0.39		1
[Si/Fe]	0.66		2	-0.06		2	0.17		2
[Ca/Fe]	0.21	0.24	12	0.04	0.19	16	0.19	0.16	17
[Sc/Fe]	-0.07	0.20	5	-0.21	0.23	4	-0.06	0.13	8
[Ti I/Fe]	0.01	0.16	8	-0.11	0.25	24	0.16	0.34	27
[Ti II/Fe]	0.03	0.19	8	-0.21	0.28	7	0.27	0.32	9
[V/Fe]				-0.27	0.18	11	-0.26	0.18	11
[Cr/Fe]	-0.37	0.19	5	-0.06	0.14	7	0.00	0.13	7
[Mn/Fe]	≤-0.70		1	-0.15	0.13	8	0.05	0.29	9
[Co/Fe]				-0.02	0.19	3	-0.18	0.12	4
[Ni/Fe]	-0.21	0.24	5	-0.16	0.26	11	-0.18	0.17	12
[Cu/Fe]	≤-0.76		1	-0.34		1	-0.38		1
[Zn/Fe]	0.09		1	-0.23		1	0.00		1
[Y/Fe]	-0.56		2	0.21	0.23	3	-0.22	0.23	3
[Zr/Fe]	≤0.26		1	0.75		1	0.04		1
[Ba/Fe]	-1.28	0.16	3	0.38		2	0.18	0.10	3
[La/Fe]				0.85	0.24	8	0.11	0.17	7
[Ce/Fe]				0.71	0.17	4	0.32	0.13	4
[Pr/Fe]				0.88	0.08	5	0.40	0.08	4
[Nd/Fe]	-0.01		2	1.00	0.24	23	0.36	0.20	19
[Sm/Fe]				1.33		2	0.33		2
[Eu/Fe]				0.97		2	0.61		2
[Gd/Fe]				1.67	0.10	3	1.00		1
[Dy/Fe]				1.52		2	0.30		2
[Er/Fe]				1.38	0.30	3			

**Table 6.** continued.

	BD +30°2611			HD 216143			M92-III-13		
	S.D.		N	S.D.		N	S.D.		N
[Fe I/H]	-1.52	0.09	74	-2.12	0.08	98	-2.18	0.12	76
[Fe II/H]	-1.51	0.08	11	-2.16	0.07	15	-2.18	0.12	11
[Na/Fe]	-0.31		2	-0.15	0.03	4	0.42		2
[Mg/Fe]	0.43		1	0.64		1	0.74		1
[Si/Fe]	0.13		2	0.24		2	0.36		1
[Ca/Fe]	0.21	0.14	17	0.26	0.09	16	0.29	0.10	16
[Sc/Fe]	-0.06	0.09	8	-0.19	0.08	7	0.08	0.07	7
[Ti I/Fe]	0.02	0.14	28	0.05	0.14	22	0.07	0.12	26
[Ti II/Fe]	0.12	0.17	9	0.04	0.14	9	0.25	0.13	9
[V/Fe]	-0.19	0.11	12	-0.27	0.18	9	-0.19	0.15	11
[Cr/Fe]	-0.21	0.13	8	-0.21	0.08	8	-0.29	0.10	8
[Mn/Fe]	-0.12	0.14	9	-0.33	0.14	9	-0.40	0.17	9
[Co/Fe]	0.03	0.04	4	-0.06	0.11	4	0.13	0.07	4
[Ni/Fe]	-0.16	0.27	12	-0.10	0.21	12	-0.14	0.21	12
[Cu/Fe]	-0.44		1	-0.75		1	-0.61		1
[Zn/Fe]	-0.15		1	0.04		1	-0.10		1
[Y/Fe]	-0.23	0.17	4	-0.29	0.05	4	-0.35	0.07	4
[Zr/Fe]	0.05		1	-0.09		1	0.02		1
[Ba/Fe]	0.07	0.05	3	-0.12	0.07	3	-0.38	0.05	3
[La/Fe]	0.37	0.10	8	-0.04	0.09	5	-0.17	0.01	3
[Ce/Fe]	0.05	0.07	4	-0.19	0.11	3	-0.46		1
[Pr/Fe]	0.28	0.15	5	0.13	0.18	4	-0.09	0.15	4
[Nd/Fe]	0.19	0.15	23	-0.03	0.12	18	-0.23	0.19	13
[Sm/Fe]	0.04		2	0.08		2	-0.24		1
[Eu/Fe]	0.48		2	0.46		2	-0.10		1
[Gd/Fe]	1.08	0.11	3						
[Dy/Fe]	1.01		1	0.72		1	0.36		2
[Er/Fe]	0.30	0.20	3						

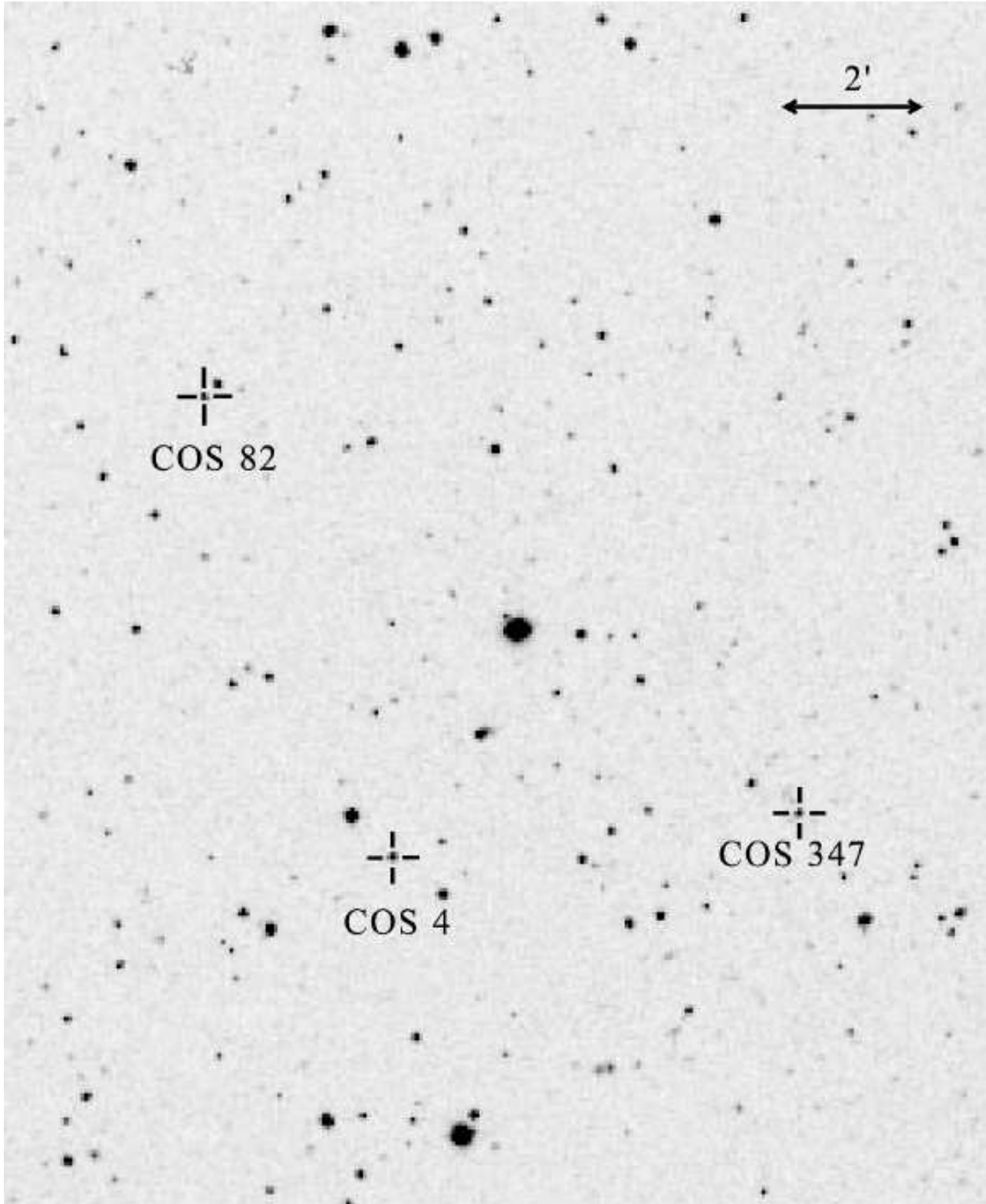


**Fig. 1.** A map of the sky area containing three target stars cos4, cos82, and cos 347. The figure is centered at R.A. (2000)  $15^{\text{h}}09^{\text{m}}10^{\text{s}}.0$  and Dec (2000)  $+67^{\circ}12'52''$ .

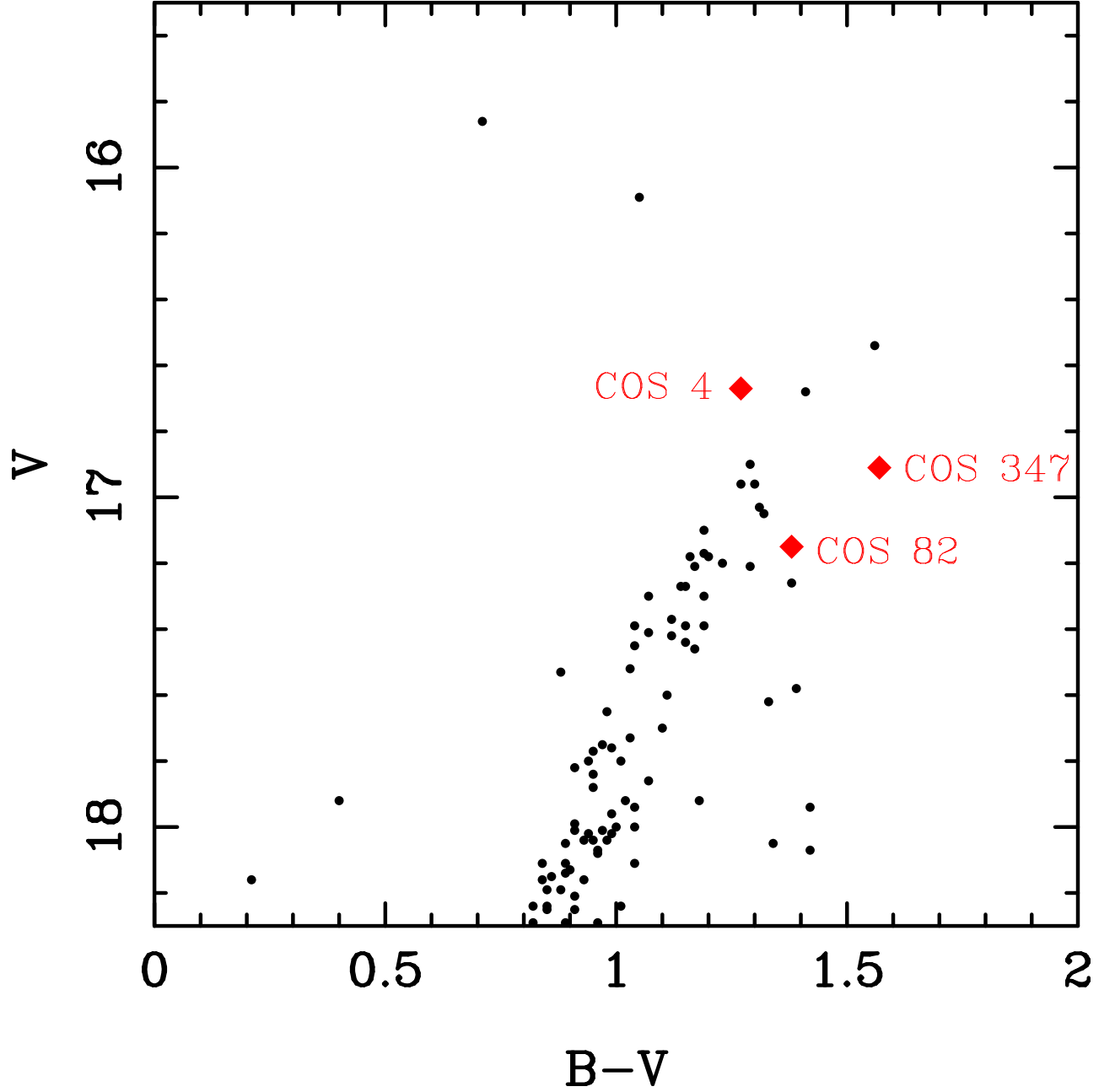


**Fig. 2.**  $B - V$  color-magnitude diagram for the UMi dSph. Only stars with the membership probability higher than 90 % are plotted on the figure. Diamond marks represent the RGB stars for which we took spectra. Photometric data and membership probability are taken from a catalogue prepared by A. Schweitzer (private communication).

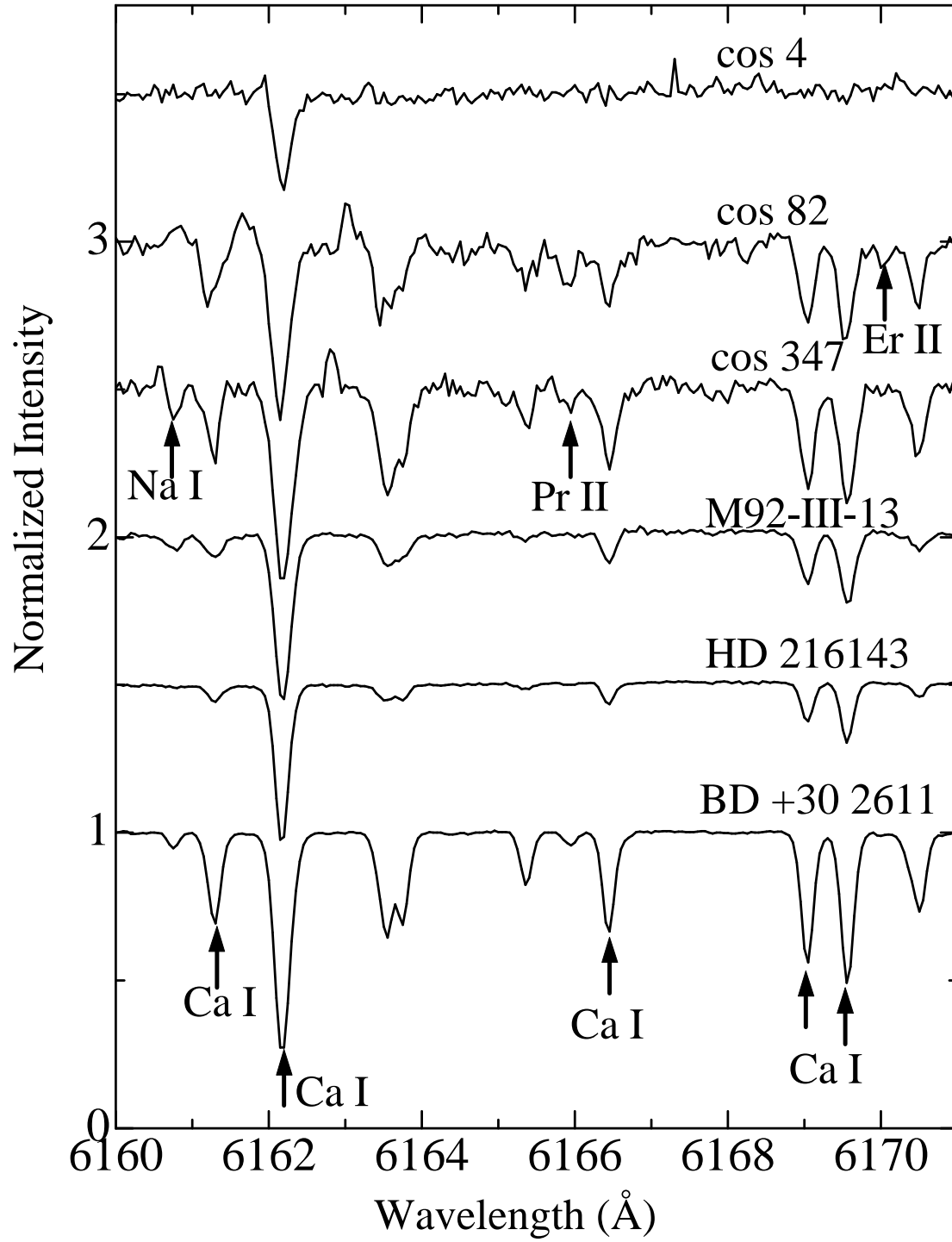


**Fig. 3.** A small portion of the observed spectra of target stars. Strong lines of Ca I are identified for the reference star BD +30°2611. Unusually strong lines of heavy rare earth elements Pr and Er are identified in cos 82. In cos 4, only one line (Ca I 6162 Å) can be detected and it suggests that the star is very metal deficient.



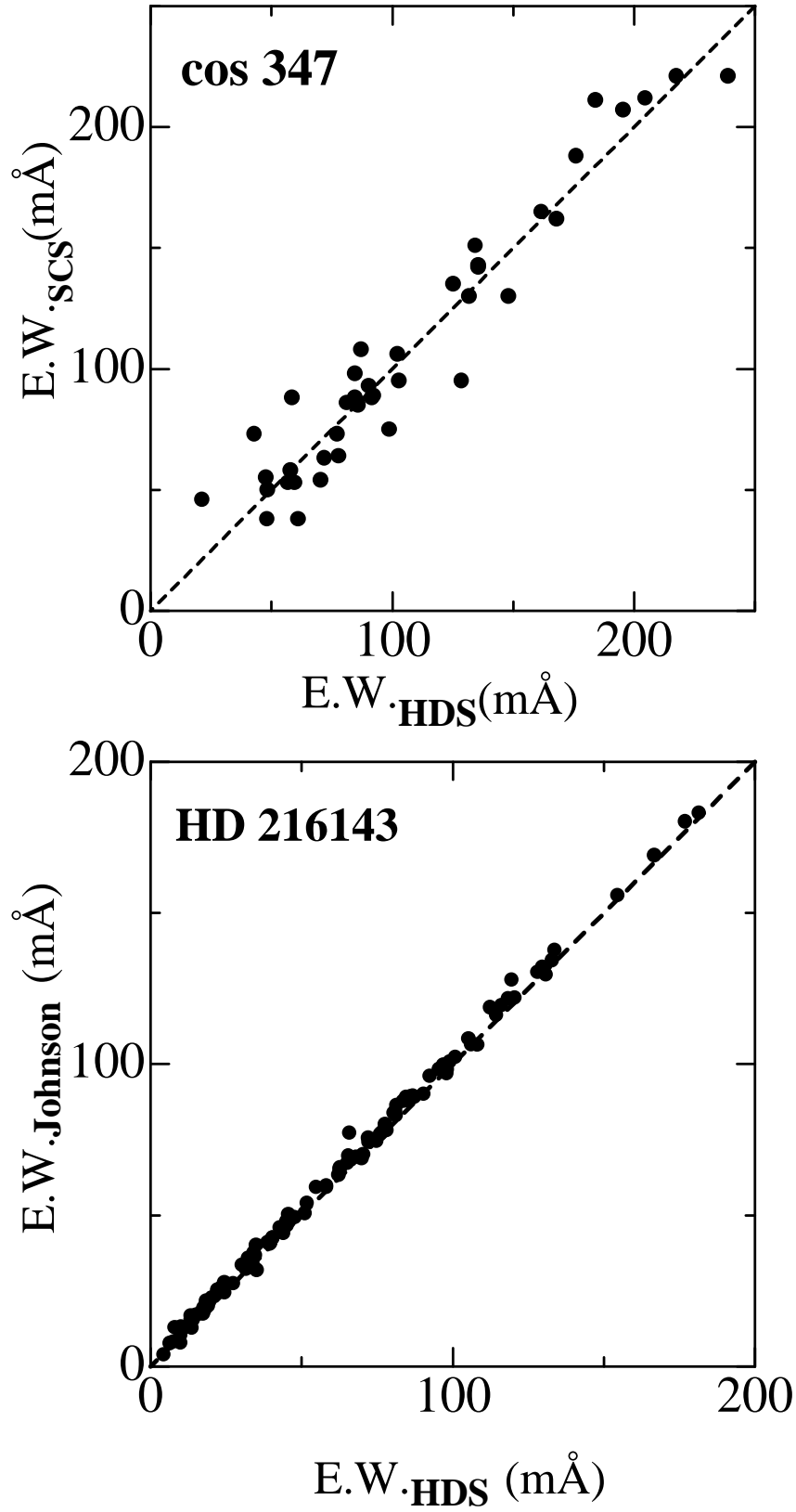


**Fig. 4.** Comparisons of observed equivalent widths. Our measurements are compared with results given in Shetrone et al. (2001) for cos 347 (upper panel) and those given in Johnson (2002) for HD 216143 (lower panel).

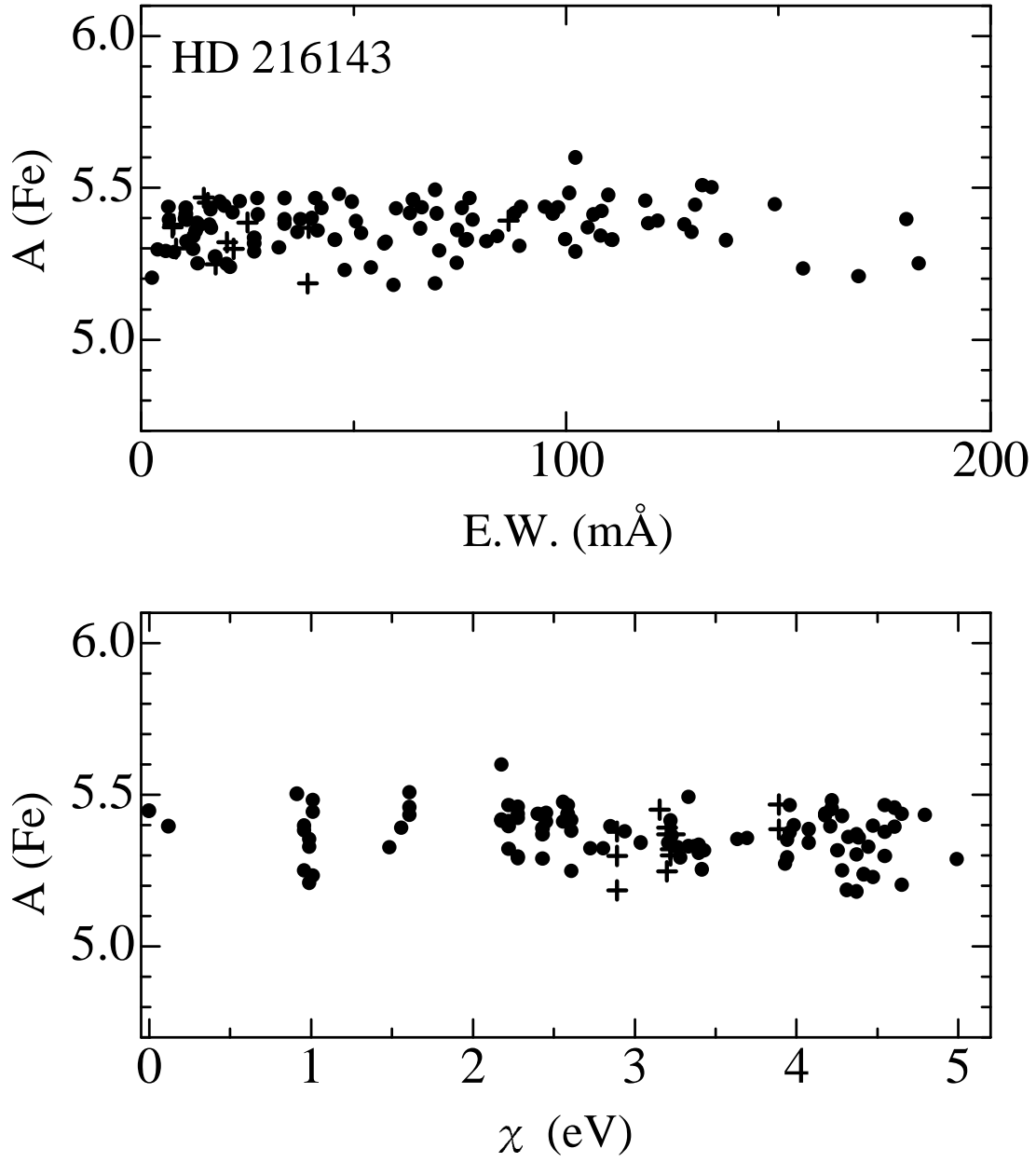


**Fig. 5.** Analyses of Fe I and Fe II lines in HD 216143. The relations between  $A(\text{Fe})$  and the equivalent widths (upper panel) and those with the lower excitation potential (lower panel) are displayed. The Fe I and Fe II lines are denoted by filled circles and plus signs, respectively.

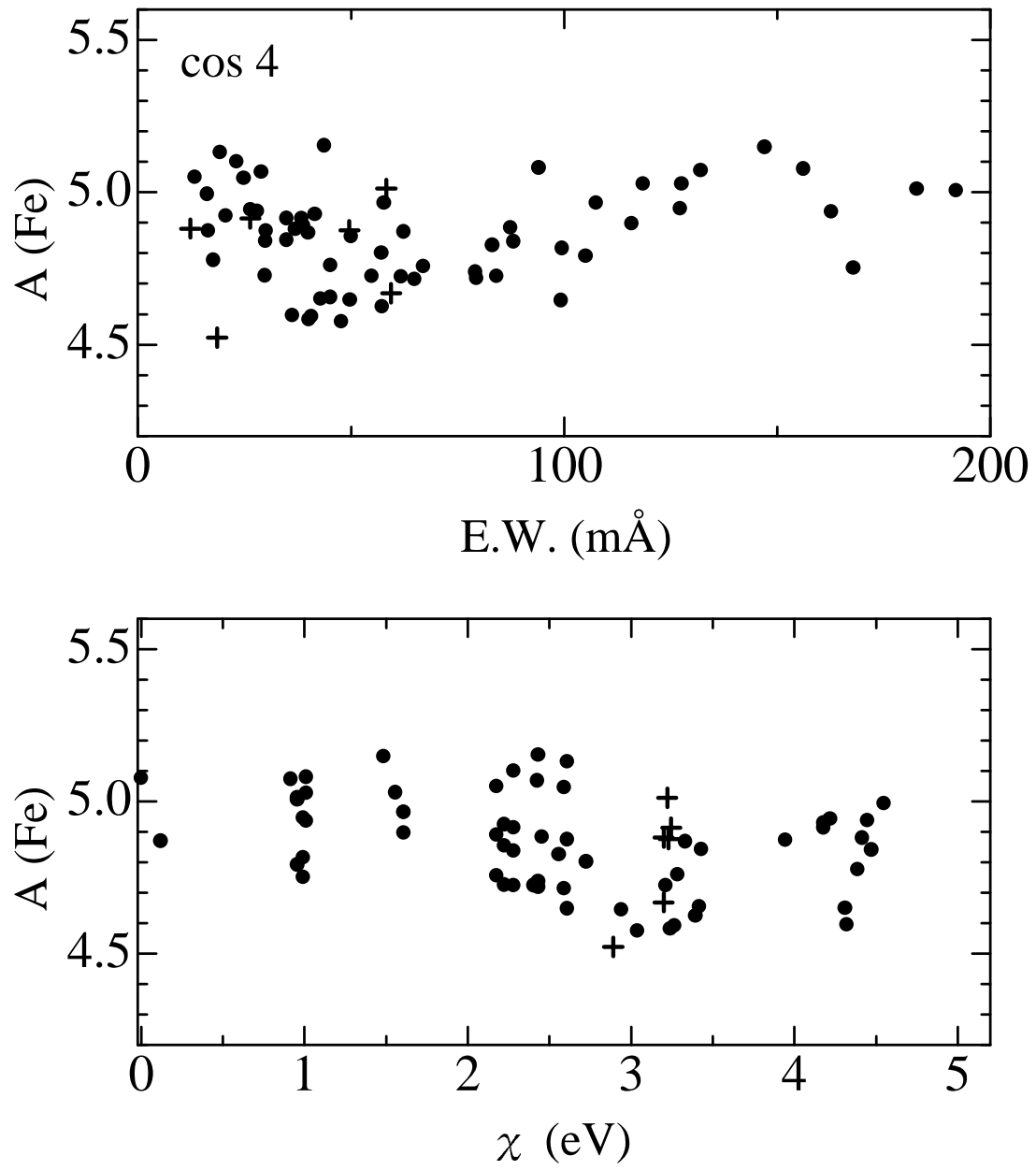


**Fig. 6.** Same as figure 3, but for cos 4

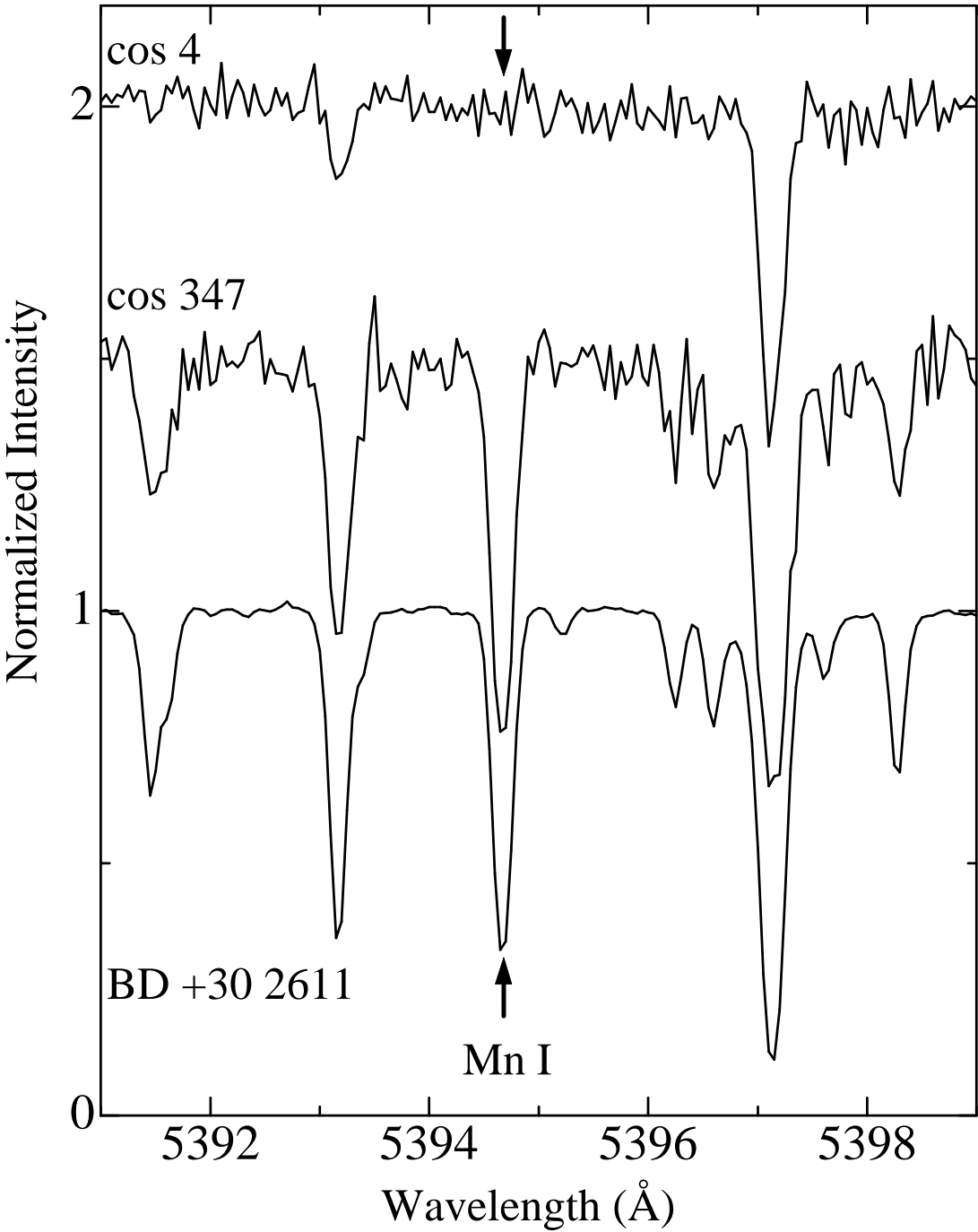


Fig. 7. The Mn I line at 5394.68 Å. Note the weakness of the line in cos 4.

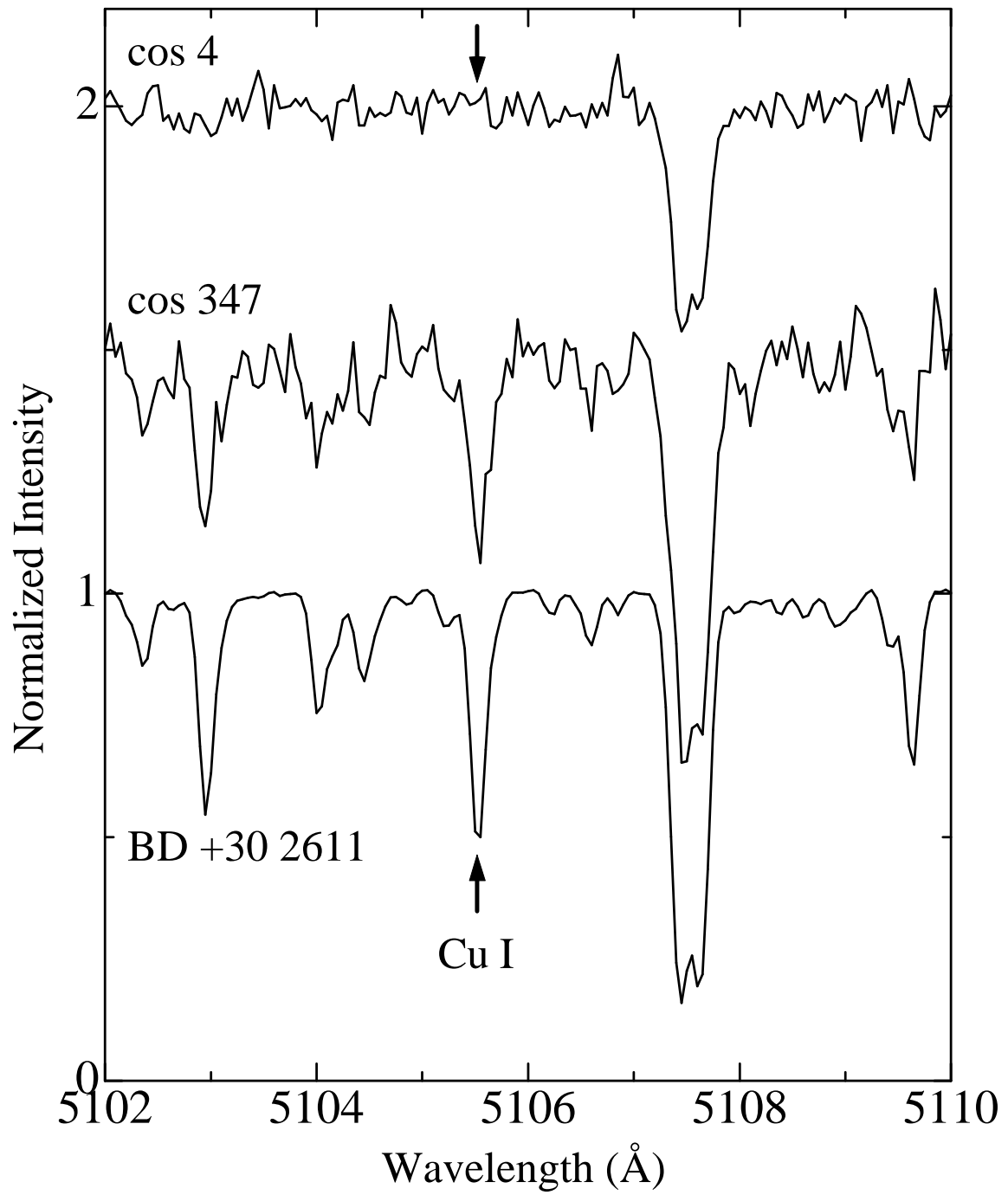


Fig. 8. The Cu I line at 5105.54 Å. Note the weakness of the line in cos 4.



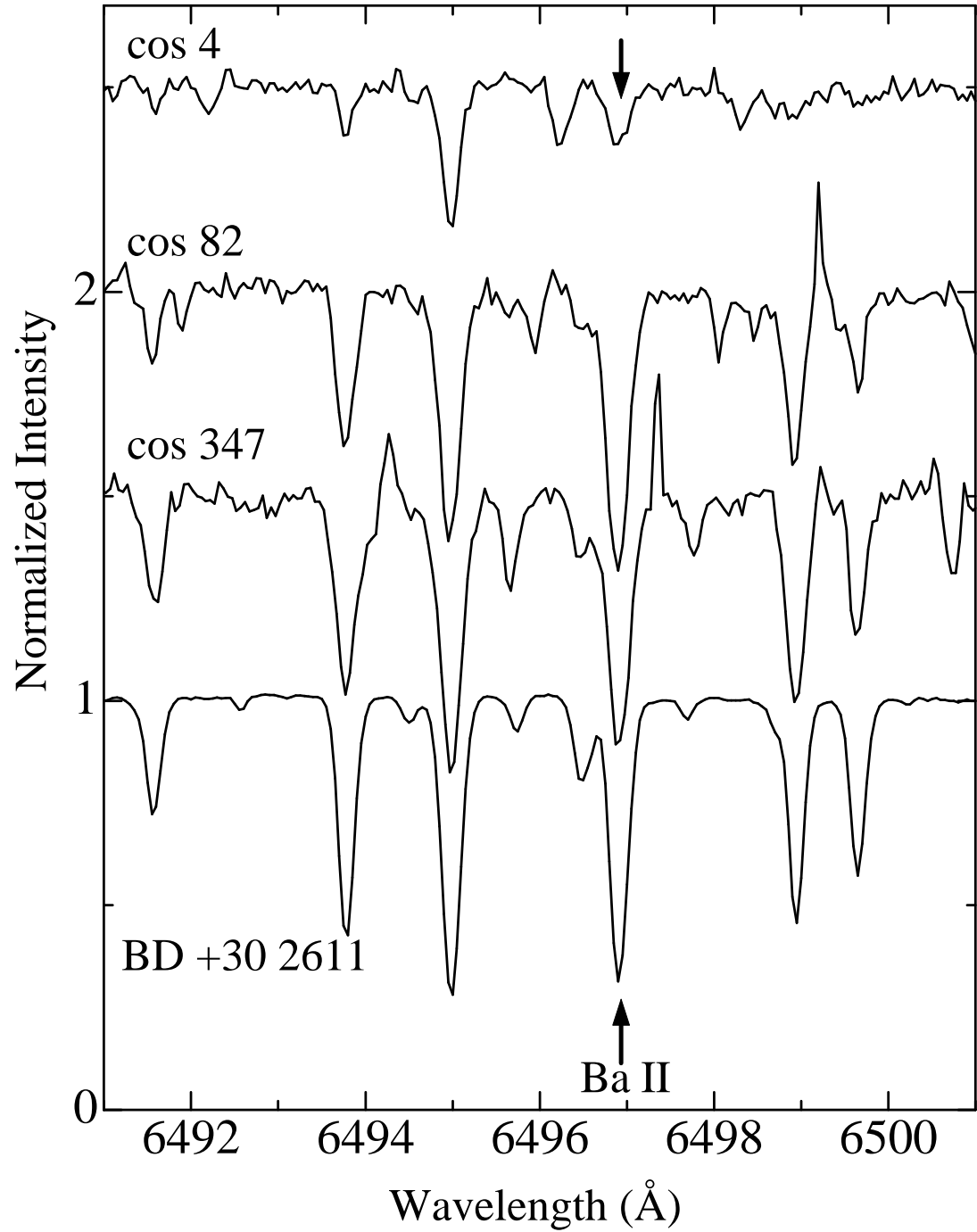


Fig. 9. The Ba II line at 6496.90 Å. Note the weakness of the line in cos 4.

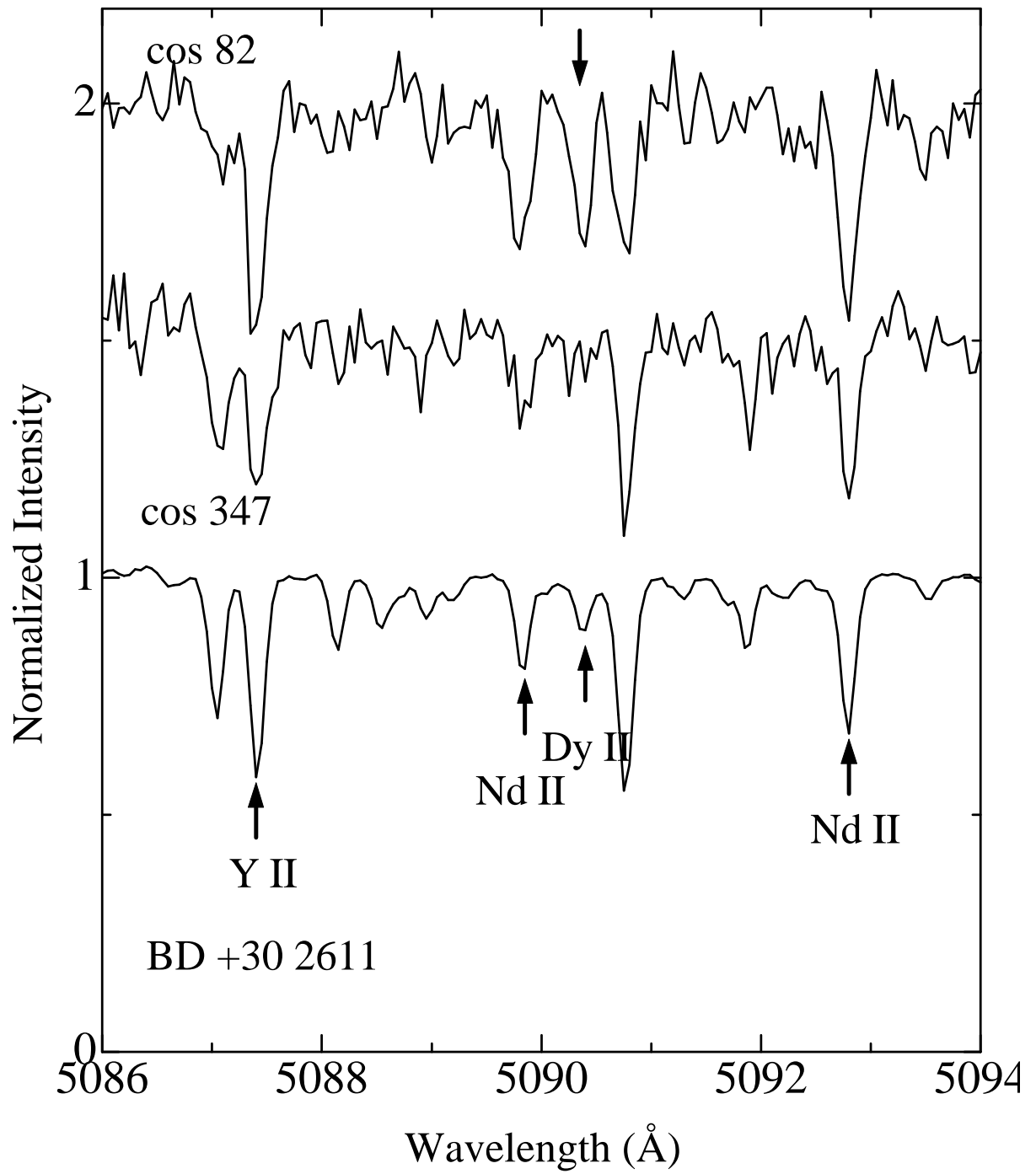
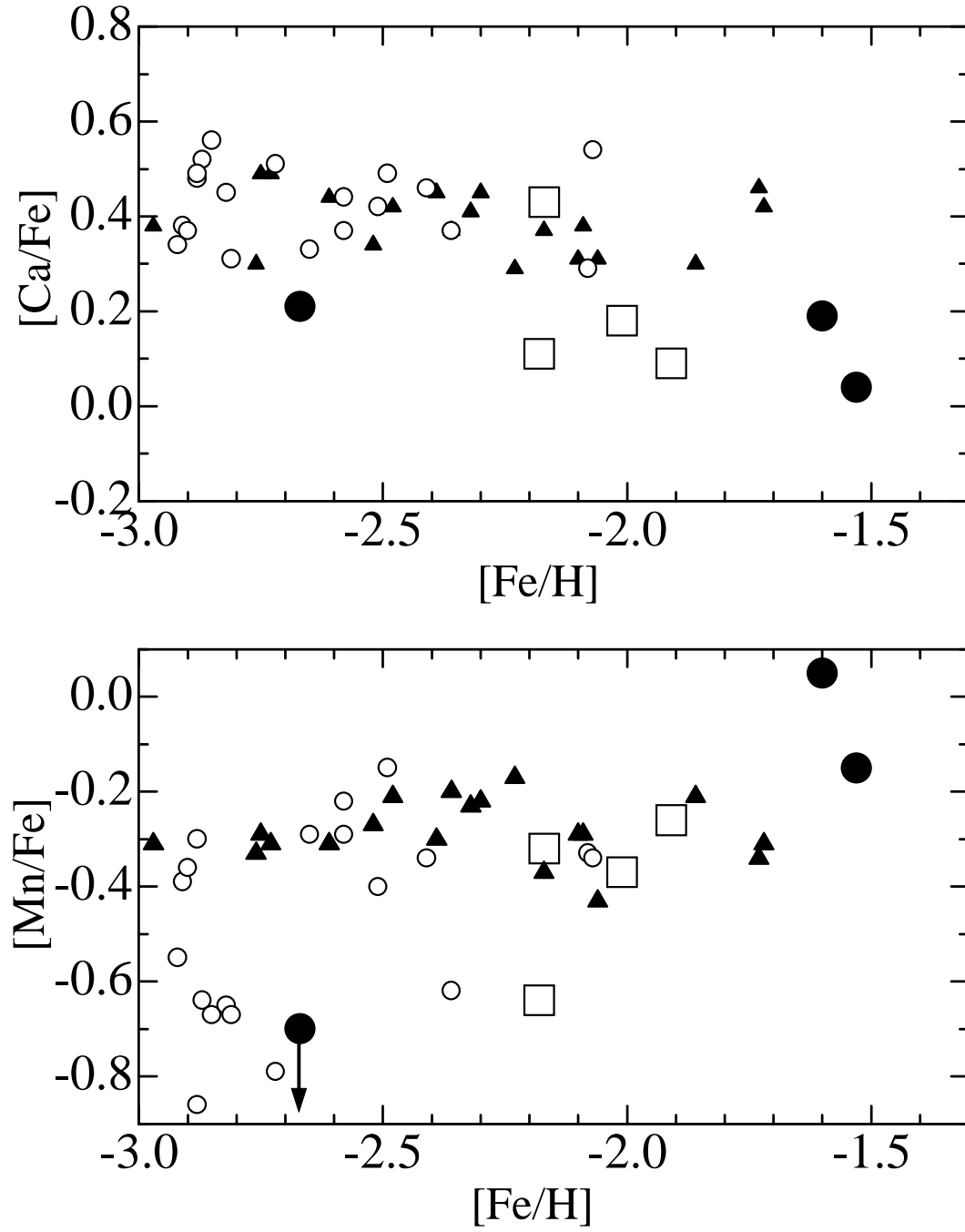
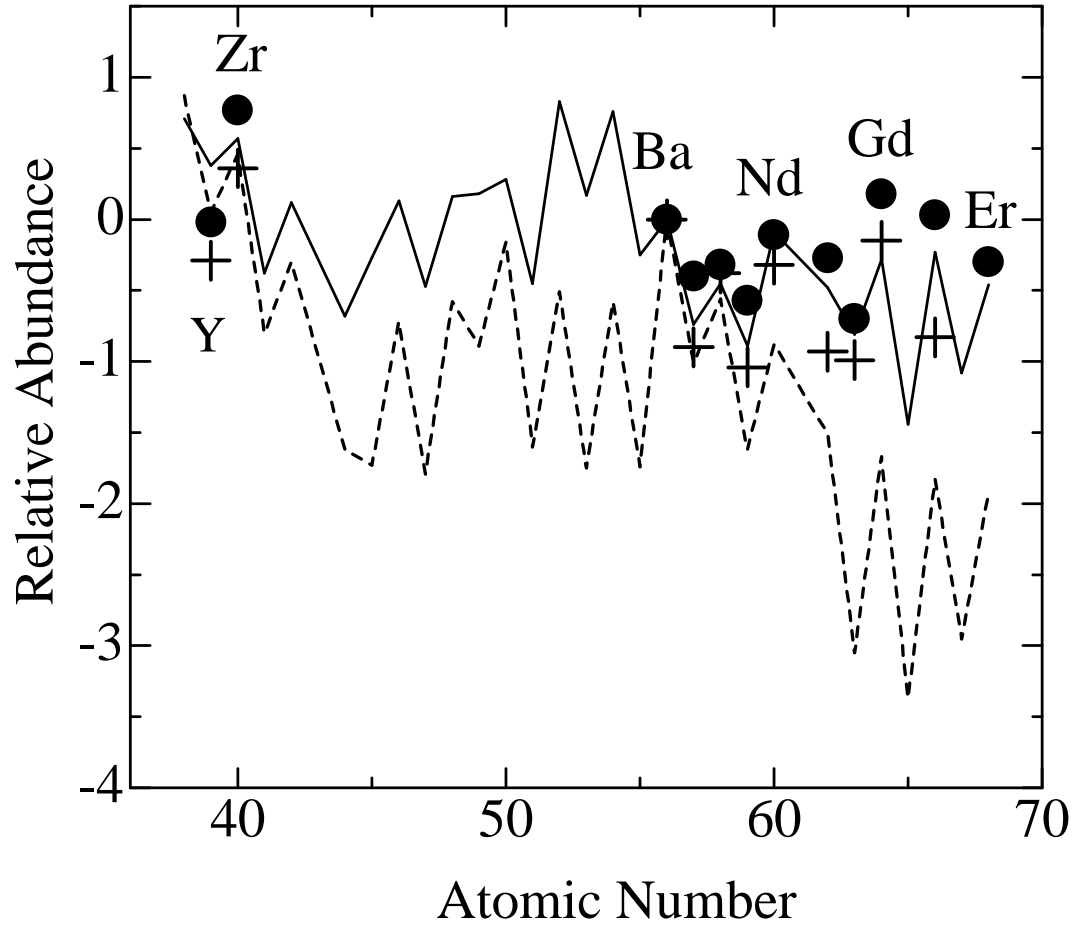


Fig. 10. The Dy II line at 5090.39 Å. The line is extraordinarily strong in cos 82.



**Fig. 11.**  $[\text{Ca}/\text{Fe}]$  vs  $[\text{Fe}/\text{H}]$  (upper panel) and  $[\text{Mn}/\text{Fe}]$  vs  $[\text{Fe}/\text{H}]$  (lower panel) relations for seven UMi stars and for galactic metal poor stars. Three UMi stars (cos 4, cos 82, and cos 347) are shown by large filled circles. Other UMi stars analyzed in Shetrone et al. (2001) are shown by large open squares. Small filled triangles and small open circles are galactic metal poor stars analyzed in



**Fig. 12.** Abundances of neutron capture elements (Y through Er) in cos 82 (filled circles) and in cos 347 (plus signs). They are compared to the scaled solar system  $r$  and  $s$ -process abundance curves, which are represented by solid and broken lines, respectively. Abundances are normalized at Ba.